Ocean Sci., 19, 1203–1223, 2023
https://doi.org/10.5194/os-19-1203-2023

Ocean Science Open Access EGU

Assessment of Indonesian Throughflow transports from ocean reanalyses with mooring-based observations

Magdalena Fritz[1,2], **Michael Mayer**[1,2,3], **Leopold Haimberger**[1], **and Susanna Winkelbauer**[1,2]

[1]Department of Meteorology and Geophysics, University of Vienna, Vienna, Austria
[2]b.geos GmbH, Industriestraße 1, 2100 Korneuburg, Austria
[3]Research Department, European Centre for Medium-Range Weather Forecasts, Reading, UK

Correspondence: Magdalena Fritz (m.fritz@univie.ac.at)

Received: 9 March 2023 – Discussion started: 14 March 2023
Revised: 16 June 2023 – Accepted: 11 July 2023 – Published: 10 August 2023

Abstract. The transport of heat and freshwater from the Pacific Ocean to the Indian Ocean via the Indonesian seas is commonly referred to as the Indonesian Throughflow (ITF). The interaction between the ITF and large-scale phenomena occurring from intraseasonal to decadal timescales reflects its connection to the global ocean and the climate system, indicating the need for monitoring the ITF region. In situ observations in this region are highly valuable, but they are temporally and spatially insufficient for near-real-time monitoring. Ocean reanalyses have the potential to serve as near-real-time monitoring tools and to extend time series backward in time, yet a comprehensive quality assessment of their realism in this region with challenging bathymetry has been lacking so far. We focus on oceanic transports diagnosed from the Copernicus Marine Service (CMEMS) Global Reanalysis Ensemble Product (GREP) and the higher-resolution product GLORYS12V1, totaling six reanalysis products. They are validated against in situ observations taken from two different monitoring programs, namely International Nusantara Stratification and Transport (INSTANT 2004–2006) and Monitoring the Indonesian Throughflow (MITF 2006–2011 and 2013–2017), resulting in a total time series of about 11.5 years in the major inflow passage of the Makassar Strait and shorter sampled time series in the Lombok Strait, the Ombai Strait, and the Timor Passage. Results show that there is reasonable agreement between reanalysis-based transports and observations in terms of means, seasonal cycles, and variability, although some shortcomings stand out. The lower-resolution products do not represent the spatial structure of the flow accurately. They also tend to underestimate the integrated net flow in the narrower straits of Lombok and Ombai, an aspect that is improved in GLORYS12V1. Reanalyses tend to underestimate the effect of seasonal Kelvin waves on the transports, which leads to errors in the mean seasonal cycle. Interannual variations of reanalyzed transports agree well with observations, but uncertainties are much larger on sub-annual variability. Finally, as an application of physically consistent and observationally constrained fields provided by ocean reanalyses, we study the impact of the vertically varying pressure gradient on the vertical structure of the ITF to better understand an apparent two-layer regime of the flow.

1 Introduction

The Indonesian seas (Fig. 1) are the primary low-latitude connection between the global oceans that allow the transport of heat and freshwater from the Pacific Ocean to the Indian Ocean (Piola and Gordon, 1984; Vranes et al., 2002; Potemra et al., 2003). This connection is known as the Indonesian Throughflow (ITF, Wyrtki, 1961). The Indonesian Archipelago is characterized by many narrow and deep straits connecting seas and basins of varying sizes and depths. The region is relevant because changes in sea surface temperature over the Indo-Pacific warm pool, where one ascending branch of the Walker circulation lies, are strongly coupled to the atmosphere and hence can modulate atmospheric circulation in the global tropics and beyond (Godfrey, 1996; Sprintall et al., 2014). Two western boundary currents prevail at the entrance of the Indonesian seas: the North Pacific Mindanao Current (Schönau et al., 2015) and the South

Pacific New Guinea Coastal Current (Cresswell, 2000). The western boundary currents collide and form the ITF as well as the retroflections that feed the North Equatorial Counter Current (Wyrtki and Kendall, 1967). Subsequently, North Pacific upper-thermocline waters make their way through the Sulawesi Sea into the Makassar Strait (∼ 250 km), which accounts for about 80 % of the volume inflow to the ITF (Gordon, 2005). In the west, the flow through the Makassar Strait is influenced by a large shelf restricting most of the transport to the 45 km wide Labani Channel. After transiting the Makassar Strait, water masses either enter the Banda Sea through the Flores Sea or directly exit into the Indian Ocean via the shallow Lombok Strait (∼ 35 km) (Boy, 1995; Sprintall et al., 2009). We note that the Lifamatola Passage represents an alternative pathway to the Makassar Strait, through which South Pacific water masses can enter the Banda Sea as well (Van Riel, 1956; Van Aken et al., 2009) . From the Banda Sea, the ITF enters the Indian Ocean through small gateways along the Nusa Tenggara island chain (Godfrey, 1996) but mainly through the Ombai Strait (∼ 37 km) (Molcard et al., 2001; Sprintall et al., 2009) and the Timor Passage (∼ 160 km) (Molcard et al., 1996; Sprintall et al., 2009).

The ITF exhibits fluctuations on a broad range of timescales, from interannual timescales associated with the El Niño–Southern Oscillation (ENSO) (Mayer et al., 2018; Mayer and Alonso Balmaseda, 2021) or the Indian Ocean Dipole (IOD) (Potemra and Schneider, 2007; Pujiana et al., 2019) to decadal climate variability and its connection to the Pacific Decadal Oscillation (PDO) (Nieves et al., 2015; Ummenhofer et al., 2017). On shorter timescales, the Madden–Julian Oscillation (MJO) (Nieva Tamasiunas et al., 2021) and the Australian–Indonesian monsoon (Clarke and Liu, 1993; Masumoto and Yamagata, 1996) strongly impact the behavior of the ITF. Related to the latter, the mean seasonal cycle of the ITF is dictated by trade winds over the western Pacific and reversing wind patterns tied to the monsoon phases, as first postulated by Wyrtki (1987). Together they maintain an inter-ocean pressure gradient between the western Pacific and the eastern Indian Ocean that regulates the ITF.

During the southeast (SE) monsoon, southeasterly winds blow along the coast of Sumatra, Java, and the Nusa Tenggara island chain, and this, as a result of Ekman transports (Ekman, 1905), pushes water masses offshore (Masumoto and Yamagata, 1996), resulting in a local mean sea level decrease. This, in turn, increases the inter-ocean pressure gradient towards the Indian Ocean and favors a stronger southward ITF transport. During boreal winter, when the northwest (NW) monsoon prevails, the opposite holds true. Accordingly, we can understand the seasonal cycle of ITF transport by studying the inter-ocean pressure gradient between the ITF's entrance and exit region, which at $z = 0$ is proportional to the sea level gradient.

Several studies successfully employed ocean reanalyses to quantify different aspects of ocean climate, e.g., volume and heat transport (Pietschnig et al., 2017), ocean heat content (Balmaseda et al., 2013; Palmer et al., 2017; Asbjørnsen et al., 2019; Uotila et al., 2019), and energy budgets (Mayer et al., 2019, 2022). In the ITF area, ocean reanalyses have also been used to study multidecadal (Ummenhofer et al., 2017) and interannual (Mayer et al., 2018) anomalies (related to, e.g., PDO, ENSO, and IOD) of transports, which regulate the Indo-Pacific heat transfer. However, the ITF region is a challenging area for reanalysis products given the complex bathymetry, and comprehensive validation in the ITF region is still lacking. Here we aim to fill this gap by studying all relevant straits of the ITF (Makassar, Lombok, Ombai, and Timor) as represented by multiple ocean reanalysis products and validation through available in situ observations. For this purpose, we employ in situ observations from the aforementioned International Nusantara Stratification and Transport (INSTANT) program (Sprintall et al., 2004), providing 3 years of data in the major inflow and outflow passages, and the Monitoring the Indonesian Throughflow (MITF) campaign (Gordon et al., 2019), providing temporally extended data for the Makassar Strait.

The rest of the paper is organized as follows: Sect. 2 introduces the data sets and the preprocessing methods. We

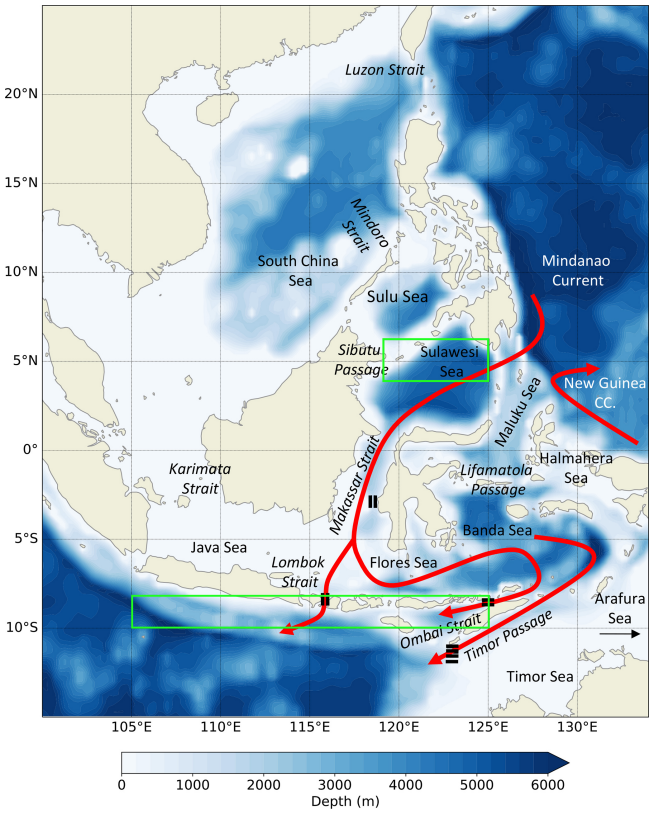

Figure 1. Study area: the Indonesian seas. Solid red arrows display schematics of the Indonesian Throughflow. Bold black lines indicate mooring sites during the INSTANT program. Green encircled areas correspond to the ITF's entrance (119–125° E, 4–6° S) and exit (105–125° E, 8–10° S) regions.

continue with a comprehensive comparison between mooring observations and six reanalysis products using suitable diagnostics in Sect. 3. Furthermore, we focus on the relation between the ITF and the vertically varying pressure gradient. Conclusions follow in Sect. 5.

2 Data and methods

2.1 Mooring data

Observational data used throughout this study were measured during the INSTANT field program (August 2003 to December 2006) in the Makassar Strait (Gordon et al., 2008), the Lombok Strait, the Ombai Strait, and the Timor Passage (Sprintall et al., 2009). Measurements continued in the Makassar Strait from December 2006 to August 2011 and from August 2013 to August 2017 (MITF Gordon et al., 2019), yielding a total of 11.5 years of observational data in the Makassar Strait. The moorings were instrumented with upward-looking acoustic Doppler current profilers (ADCPs) and various current meters to measure zonal (u) and meridional (v) velocities, as well as temperature, salinity, and pressure (Cowley et al., 2009). In order to obtain along-strait velocities, we employed the following preprocessing routine: first, we resample the data onto a common time base of 2 h and deal with missing velocities, which mostly occurred in the surface layer, as follows. As in Sprintall et al. (2009), gaps were filled using linear interpolation or constant velocity equal to the shallowest measured velocity, i.e., nearest vertical neighbors. A data set for each mooring is then created by linearly interpolating the observations to the vertical levels as defined in the reanalysis products. Measurements from ADCPs require special treatment to account for mooring blow-over. Thus, we determine the actual measuring depths by subtracting the ADCP's range of bins from its location at each time stamp, as given by the pressure time series. We choose the lowest measured pressure value and assume it to be the mooring's depth at rest. That followed, we compiled data sets for the u and v components (as measured by the current meters) and generated along-strait velocities (ASVs) by projection of their contribution onto the along-strait vector $\boldsymbol{n}$.

According to Gordon et al. (2008) and Sprintall et al. (2009), the orientation of the along-strait vector $\boldsymbol{n}$ can be determined in several ways. We use a geometric approach, independent of any measurements (e.g., pressure gauges). Since the moorings within a strait are almost all aligned perpendicular to the strait, $\boldsymbol{n}$ is defined as the vector normal to the direction vector between the two outermost mooring locations. Accordingly, the along-strait velocity is the sum of the projections of u and v on $\boldsymbol{n}$. To estimate the transport through each strait, the velocity profiles at each mooring site are laterally interpolated (within 10 m bins) between each other and extrapolated to the sidewalls. The interpolation–extrapolation is performed within the bathymetry as specified by the $1/4°$ (Fig. 2a) and $1/12°$ (Fig. 2b) reanalysis products while assuming a linear drop-off to zero towards the shore. Integration over the cross-passage interpolation of ASVs yields mean volume transports.

Significant gaps occur for the Timor Sill data from August 2004 to June 2005 and during the second deployment, where data are only available between $\sim$ 300–1900 m. Since only the west mooring was operational during the MITF program (2006–2017), velocity data at the eastern site were estimated using a linear regression model, which was motivated by the high correlation of velocities measured at the east and west mooring during the INSTANT period. Also, observational data for the INSTANT period were preprocessed as mentioned above, while MITF data were downloaded and fully preprocessed, without detailed documentation of the methods (our technique closely follows the processing described in Gordon et al., 2008; Sprintall et al., 2009). We apply the same correlation-based approach to the Lombok west mooring, where data are unavailable after June 2005 due to an early mooring parting. Data output from individual instruments that exhibited significant gaps or stopped working entirely was generally not considered.

2.2 Reanalysis data

We evaluated the following reanalysis products: Euro-Mediterranean Center on Climate Change (CMCC) Global Ocean Physical Reanalysis System (CGLORS) (Storto and Masina, 2016), Forecasting Ocean Assimilation Model (FOAM) (MacLachlan et al., 2015), Global Ocean Reanalysis and Simulation Version 4 (GLORYS2V4) (Garric and Parent, 2017), Ocean Reanalysis System 5 (ORAS5) (Zuo et al., 2015), and Ocean ReAnalysis Pilot system-6 (ORAP6) (Zuo et al., 2021). These products use the NEMO ocean model (Madec et al., 2008) in the ORCA025.L75 (Madec and Imbard, 1996) configuration, indicating an eddy-permitting horizontal resolution of $1/4° \times 1/4°$ ($\sim$ 28 km near the Equator) and 75 vertical levels. The first four products (excluding ORAP6) contribute to the Copernicus Marine Service (CMEMS) Global Reanalysis Ensemble Product (GREP) (Desportes et al., 2017); however, in this work, we also consider ORAP6 a contributor to our (extended) GREP mean. Different versions of the NEMO model are implemented as a tripolar ORCA grid with Arakawa C-grid staggering (Arakawa and Lamb, 1977), where individual variables are computed at different grid points with scalars defined at the cell center and vector components defined at the cell edges. The sixth considered product GLORYS12V1 (Lellouche et al., 2018) is also based on the NEMO model but with a increased horizontal resolution of $1/12° \times 1/12°$ ($\sim$ 9 km near the Equator) and 50 vertical levels. Within the upper 200 m, the $1/4°$ products provide data on 31 unevenly distributed vertical levels, whereas in GLORYS12V1, there are 25 levels. The considered reanalysis products employ different data assimilation methods (Table 1), assimilating satel-

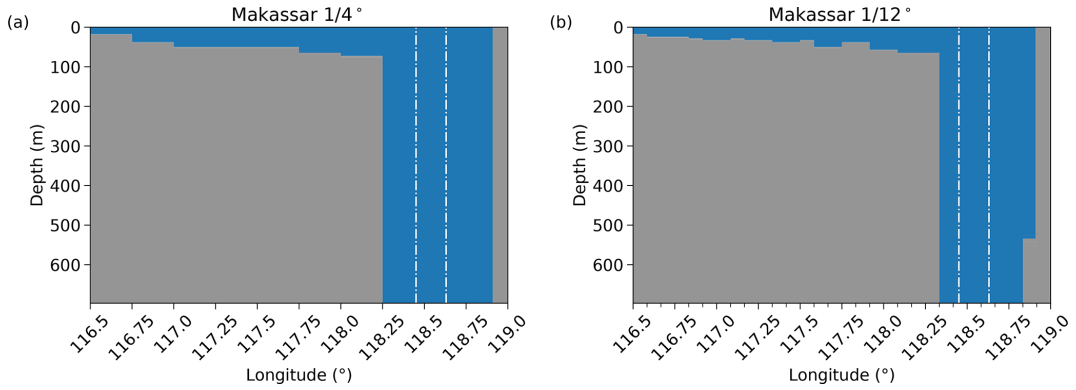

Figure 2. Bathymetries for the cross-passage interpolation of ASVs as given by the **(a)** $1/4° \times 1/4°$ (75 levels) and **(b)** $1/12° \times 1/12°$ (50 levels) products in the Makassar Strait. White dash–dot lines represent mooring locations.

Table 1. Product name (institution), resolution (horizontal and vertical), ocean model (version), atmospheric forcing, and data assimilation method for the considered reanalyses.

Product	Resolution	Ocean model	Forcing	Data assimilation
C-GLORS (v7) (CMCC)	ORCA025.L75	NEMO (v3.6)	ERA-Interim	3D-Var/FGAT (OceanVar[1])
FOAM (Met Office)	ORCA025.L75	NEMO (v3.2)	ERA-Interim	3D-Var/FGAT (NEMOVAR[2])
ORAS5 (ECMWF)	ORCA025.L75	NEMO (v3.4)	ERA-Interim	3D-Var/FGAT (NEMOVAR)
ORAP6 (ECMWF)	ORCA025.L75	NEMO (v3.4)	ERA5	3D-Var/FGAT (NEMOVAR)
GLORYS2V4 (Mercator Ocean)	ORCA025.L75	NEMO (v3.1)	ERA-Interim	Kalman filter (SAM[3])
GLORYS12V1 (Mercator Ocean)	ORCA12.L50	NEMO (v3.1)	ERA-Interim	Kalman filter (SAM)

[1] Dobricic and Pinardi (2008). [2] Mogensen et al. (2012). [3] Lellouche et al. (2018).

lite observations of sea level anomalies, in situ observations of sub-surface temperature and salinity, and remotely sensed sea ice concentration (SIC) and sea surface temperature (SST). In situ observations are extracted from the quality-controlled UK Met Office EN4 data sets (Good et al., 2013) or the CORA data set from the Institut Français de Recherche pour l'Exploitation de la Mer (IFREMER) (Cabanes et al., 2013), which include a huge collection of in situ profiles of temperature and salinity. We note that coverage by Argo profiling floats (Argo, 2000) is limited in the ITF region; i.e., observational coverage is reduced in the ITF compared to other tropical regions. Also note that current measurements from mooring buoys are not assimilated, which makes the intercomparison with in situ observations of oceanic currents completely independent. The ECMWF ERA-Interim atmospheric reanalysis (Dee et al., 2011) is used to force each of the reanalyses at the surface using CORE bulk formulas (Large and Yeager, 2004), except ORAP6, which employs updated forcing based on ERA5 (Hersbach et al., 2020).

Since all products use Arakawa C-grid staggering, the definition of an ASV vector is not straightforward. The procedure yielding cross-sections of ASVs follows that of the observations; however, the projection from the native grid onto the geographic coordinates in the desired strait requires the implementation of three cross-products and, again, a projection of the direct velocity vectors $\boldsymbol{u}$ and $\boldsymbol{v}$ onto the along-strait vector $\boldsymbol{n}$.

3 Comparison between observations and reanalyses

3.1 Vertical profiles

We begin with an intercomparison of mean vertical profiles of ASVs in the Makassar Strait (Fig. 3). Understanding dif-

ferences in the depiction of velocity profiles between the observations and reanalysis products is essential for the interpretation of differences between them. The GREP profiles correspond to the nearest-neighbor profiles of the west and east mooring site. GLORYS12V1 west coincides with the second nearest neighbor due to a shelf-induced artifact that apparently corrupts the true nearest-neighbor profile (not shown). Due to this artifact in GLORYS12V1, the longitude (118.5° E) of the chosen vertical profile coincides with that of the GREP products.

Vertical profiles of ASV indicate stronger transport to the west of Labani Channel in observations, which is also evident in the reanalysis products, however, greatly overestimated by up to $-0.56\,\mathrm{m\,s^{-1}}$. Observations display a mean maximum velocity of $-0.54\,\mathrm{m\,s^{-1}}$ in $\sim 110\,\mathrm{m}$, while the GREP mean exhibits almost twice as high velocities with up to $-0.97\,\mathrm{m\,s^{-1}}$ in $\sim 130\,\mathrm{m}$. The lower-placed maximum is featured in all considered reanalysis products. The best agreement in terms of maximum currents is found in GLORYS2V4 ($v_{\max} = -0.71\,\mathrm{m\,s^{-1}}$). It also exhibits the highest spatial correlation ($r = 0.97$) with the observed vertical ASV profiles (as a measure of the realism of their vertical structure). The maximum velocity in GLORYS12V1 ($-0.85\,\mathrm{m\,s^{-1}}$) is weaker than in the GREP mean and thus closer to observations but still noticeably overestimated. In addition, the spatial correlation of the mean ASV profiles is lower for GLORYS12V1 ($r = 0.77$) compared to the GREP products and substantially lower than its lower-resolution counterpart GLORYS2V4. We note that we disregard the top 40 m in the computation of the correlation coefficients due to surface reflection contamination in the observations that might adulterate the correlation results (Sprintall et al., 2009; Gordon et al., 2019). At depths greater than $\sim 400\,\mathrm{m}$, reanalysis products approach near-zero velocities faster than indicated by the observations. The flow that is too weak in GREP at greater depths is even more pronounced in the eastern profiles (Fig. 3b), where observations display substantial magnitudes down to $\sim 500\,\mathrm{m}$. Qualitatively, mean reanalysis-based vertical profiles at the eastern mooring site do not exhibit such a striking deviation of peak flow from observations. However, correlation coefficients [0.8; 0.95] are similar to those for the western mooring because the vertical displacement ($\sim 20\,\mathrm{m}$) of maximum velocity in the reanalysis products remains, while the observed maximum amounts to $-0.46\,\mathrm{m\,s^{-1}}$ in $\sim 110\,\mathrm{m}$. The GREP mean displays a maximum value of $-0.54\,\mathrm{m\,s^{-1}}$, surpassed by both GLORYS products ($v_{\max_{\mathrm{GLORYS2V4}}} = -0.62\,\mathrm{m\,s^{-1}}$, $v_{\max_{\mathrm{GLORYS12V1}}} = -0.6\,\mathrm{m\,s^{-1}}$). While ORAS5 and ORAP6 draw the GREP mean profile towards lower velocities, GLORYS2V4 and GLORYS12V1 act to increase its magnitude at the eastern mooring site, which is the other way around compared to that at the western location. Velocities from reanalyses below $\sim 400\,\mathrm{m}$ decrease more strongly in all products than in observations, which influences further results as well.

3.2 Cross-sections (spatially)

Figure 4 represents cross-sections of temporally averaged (2004–2017) ASVs for the Makassar Strait. It shows that the location of the stronger core of the western mooring in the Makassar Strait is not as well resolved by the GREP mean (Fig. 4b) as in GLORYS12V1 (Fig. 4f). This most likely corresponds to the increase in available horizontal grid points in GLORYS12V1 and hence to the fact that the flow exhibits a richer structure. The observed western intensification of the flow through the Labani Channel in Fig. 4a is consistent with findings by Gordon et al. (2008). In fact, we found cross-strait differences in the strength of the flow through most of the straits (Fig. A2): in the Lombok Strait, the western side is stronger than the east, and in the Ombai Strait, the southern side carries nearly the complete transport through this strait (Sprintall et al., 2009). The 1/4° products struggle to resolve such asymmetries in the flow through the passages. The comparatively low root mean square difference (RMSD) between the cross-sections from the individual reanalysis products and the GREP mean (not shown) justify the frequently used comparison between observations and the GREP mean. Moreover, the standard deviations of the individual products around the GREP mean (Fig. 4d) are lower (RMSE $\sim 0.05\,\mathrm{m\,s^{-1}}$) than the differences between the GREP mean and the observations. As for the magnitude and depth of the strongest southward flow, reanalyses overestimate maximum velocities in the Makassar Strait and shift the core downward and too far east, as already indicated in Fig. 3. Similar differences occur in the other passages, where maximum velocities tend to be overestimated in broader and underestimated in narrow straits, respectively (Table 2). The higher-resolving bathymetry (Fig. 4e–g) leads to better agreement between observations and GLORYS12V1 as indicated by the RMSE in Fig. 4g. Furthermore, the difference plots in Fig. 4c and g emphasize that not only the 1/4° products but also GLORYS12V1 exhibit currents that are too weak at greater depths. Cross-sections for the other considered straits are provided as Appendix (Fig. A2).

3.3 Long-term mean integrated transports

The cross-sections of ASVs form the basis for the computation of integrated transports. Cross-passage interpolation of ASVs within the GREP bathymetry (1/4°, Fig. 2a) yields integrated volume transports (Table 2) of −9.9 and −10.6 Sv for the observations and the GREP mean, respectively. In comparison, within the 1/12° bathymetry (Fig. 2b), volume transports amount to −9.1 Sv for observations and −9.2 Sv for GLORYS12V1. The interpolated transport over the western shelf amounts to −1.5 Sv in the GREP mean, but remains > −1 Sv in the observations and GLORYS12V1. Our observational results for both bathymetries are lower than the values obtained by Gordon et al. (2019) (−12.5 Sv between 2004 and 2017 and −11.6 Sv for the INSTANT

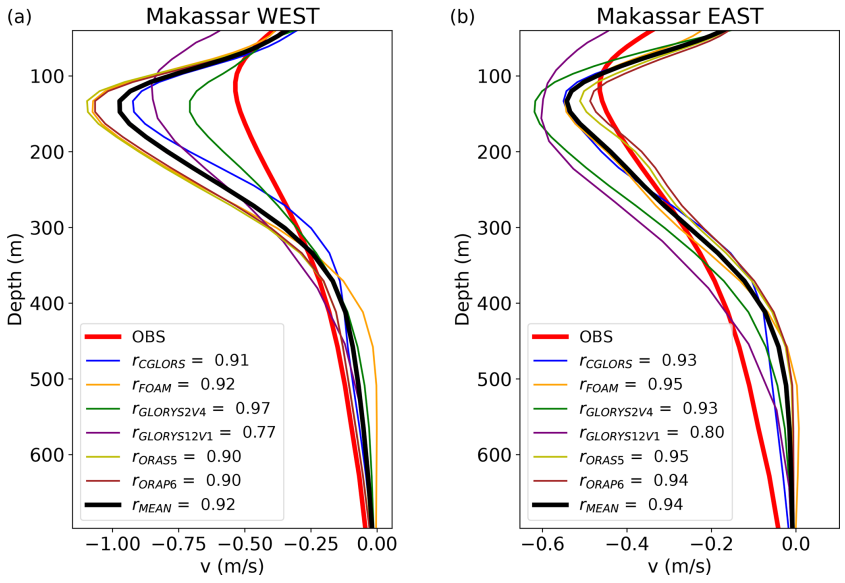

Figure 3. Mean ASV profiles for **(a)** Makassar west and **(b)** Makassar east. Purely spatial Pearson correlation coefficients between observation-based and reanalysis-based temporally averaged ASV profiles across depth are given in the boxes on the lower left. Negative values indicate southward-directed velocities (towards the Indian Ocean).

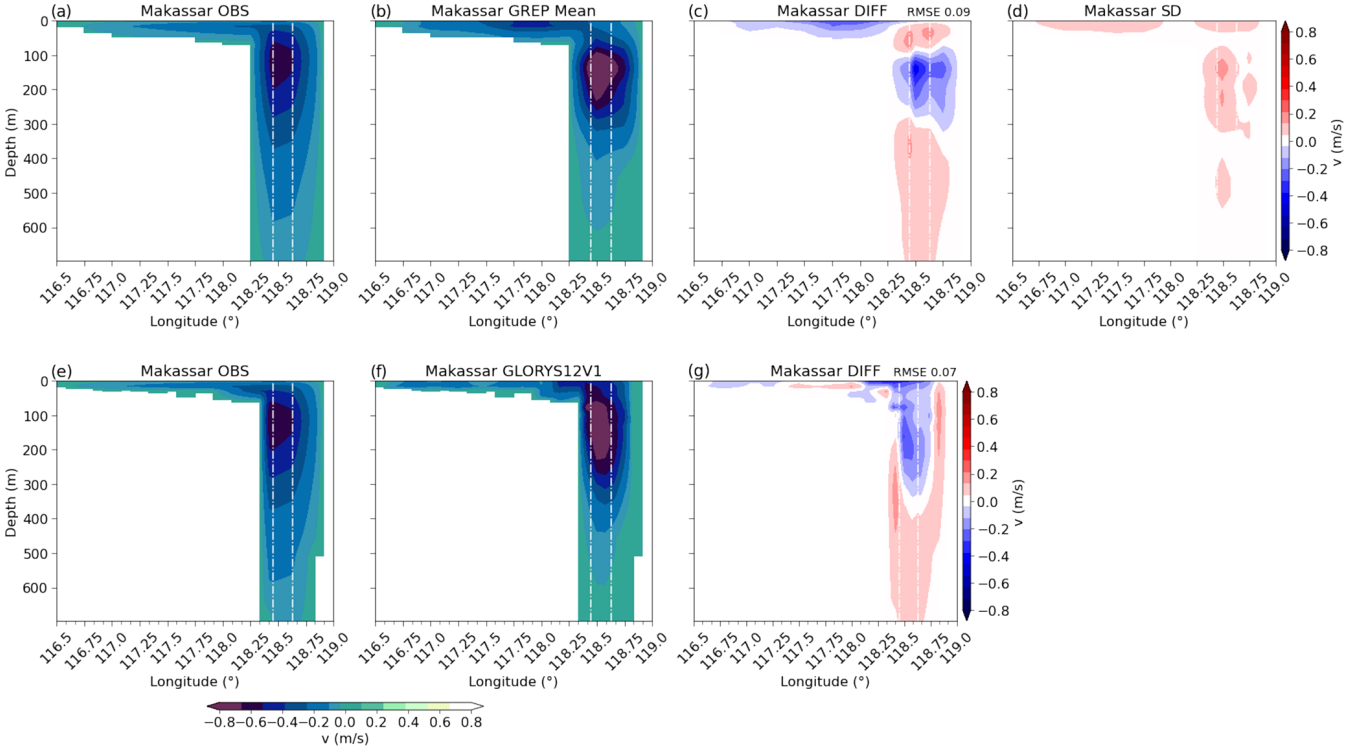

Figure 4. Mean ASV cross-sections for the Makassar Strait as given by **(a, e)** the observations, **(b)** the GREP mean, and **(f)** GLORYS12V1 for the 1/4° (upper panel) and the 1/12° (lower panel) bathymetry. Panels **(c)** and **(g)** correspond to the respective differences between observations and reanalyses with the RMSE given in the top right corner. The standard deviation of the individual products around the GREP mean is shown in **(d)**. White dash–dot lines represent mooring locations. Negative values indicate southward-directed velocities (towards the Indian Ocean).

period Gordon et al., 2008). It is however unclear which bathymetry was used in those studies. We view the implemented bathymetries in the employed products as realistic, but representation of small-scale features and precise sill depths is likely limited by the resolution of the reanalyses. Also, experimentation with the cross-passage interpolation method revealed that results strongly depend not only on the choice of bathymetry but also on assumptions about boundary conditions. Hence, the difference between our observation-based results and those from Gordon et al. (2008) likely reflect uncertainties arising from the extrapolation of two measured profiles to a complete section across one strait.

Mean transports provided in Table 2 highlight the better agreement (smaller discrepancies Δ) between the observations and GLORYS12V1 (compared to the GREP) brought forward by the $1/12°$ bathymetry, especially in Makassar ($\Delta_{1/12°} = 0.1$ Sv compared to $\Delta_{1/4°} = 0.7$ Sv) and the Lombok Strait ($\Delta_{1/12°} = 0.1$ Sv compared to $\Delta_{1/4°} = 1.1$ Sv). Taking into consideration that observed transport through Makassar is three times as strong as through Lombok, GLORYS12V1 seems to be able to accurately reproduce stronger and weaker mean velocities in both narrow and broad straits, respectively. Less obvious but still present, we find higher agreement between the observations and GLORYS12V1 in the Ombai Strait ($\Delta_{1/12°} = 1.1$ Sv) as well. Interestingly, discrepancies between observations and reanalyses in the Timor Passage seem to be smaller when considering the $1/4°$ values ($\Delta_{1/4°} = 2.2$ Sv). However, it is evident that differences between observations and reanalyses are relatively large for both bathymetries, but they seem to be emphasized for the higher-resolution bathymetry ($\Delta_{1/12°} = 2.8$ Sv). Sprintall et al. (2009) discussed results from the three outflow passages and found mean integrated transport estimates of -2.6 Sv in the Lombok Strait, -4.9 Sv in the Ombai Strait, and -7.5 Sv in the Timor Passage, which is in good agreement with our observation-based estimates.

By considering only the nearest neighbors (NNs) or interpolated profiles (INT) in Fig. 4b and f (instead of all available grid points), we can quantify how much information is lost by only observing at two sites and if the choice of mooring location represents the throughflow well. In the case of INT, we interpolated the NN to the actual mooring site in order to avoid using a NN twice in the narrow straits. The results show that the agreement between observations and the GREP mean (NN/INT) improves considerably ($\Delta_{1/4°} = 0.2$ Sv) in Makassar. The strongly pronounced maximum in the west in GLORYS12V1 leads to an exaggeration of ITF transport ($\Delta_{1/12°} = 1.7$ Sv), but it also shows that the strongest flow is indeed captured by the moorings. The additional information from the grid points in the east is thus required to keep the integrated transport inbound, a result of the biased horizontal structure of the currents in the reanalysis. Overall, the differences between considering all available grid points and using only the NN/INT values amount to ~ 10 % in all straits. Thus, we consider this to be an appropriate representation of the sampling error for the limited number of moorings. The fact that the agreements between observations and GREP/GLORYS12V1 and the agreements between observations and GREP (NN/INT)/GLORYS12V1 (NN/INT) vary in all considered straits (Table 2) highlights biased structures in the flow of the reanalyses and the need for an accurate representation of asymmetries by the reanalyses.

3.4 Mean annual cycle

The mean annual cycle of ITF transport strongly depends on the Australian–Indonesian monsoon and, thus, on seasonal variabilities in the sea level differences between the western Pacific and the eastern Indian Ocean (Wyrtki, 1987; Clarke and Liu, 1994). Sea level differences, and hence transports, are at a maximum (higher in the western Pacific) in boreal summer during the SE monsoon, while minimum transports prevail during boreal winter (NW monsoon). Due to the differences in sea level, a pressure gradient between the Pacific Ocean and the Indian Ocean establishes, which ultimately drives the ITF. As will be discussed in Sect. 4, vertically varying pressure gradients regulate the throughflow all the way to the sea floor. Thus, ITF transport through the Makassar Strait exhibits a strong vertically varying annual cycle as shown in Fig. 5a. The surface layer flow and the stronger subsurface flow in $\sim$ 100–120 m increase around July, and we find a second maximum around February–March, which is, however, less pronounced in the surface layer. The GREP mean (Fig. 5b) captures the seasonal cycle of the surface layer flow as well as the stronger subsurface core. In both layers, ASVs are considerably larger, explaining the negative differences (OBS – GREP mean) in Fig. 5c. The difference maximum around March highlights the overly high ASVs in the GREP mean between February and mid-April.

During the monsoon transition months (April to May and October to November), the vertical structure in the Makassar Strait changes, and weak ASVs (even positive) dominate lower layers. Such decreases in the throughflow represent the intrusion of Indian Ocean Kelvin waves that originate from anomalous wind forcing in the equatorial Indian Ocean and propagate along the southern coast of Sumatra and Java into the Makassar Strait via the Lombok Strait (Sprintall et al., 2000), which act to reduce ITF transport by weakening the inter-ocean pressure gradient (Gordon et al., 2019). Hovmöller plots indicate that Kelvin waves seem to appear in deeper layers first before influencing the ITF in the upper layer (Sprintall et al., 2009). Reanalyses generally have weaker flow at greater depths, and the Kelvin wave signal (marked by positive ASVs in lower layers) appears suppressed in the ASVs from reanalyses. This also has some influence on the annual cycle as discussed next with respect to Fig. 6.

The condensed view of the mean annual cycle of vertically integrated transports in Fig. 6a–d enables an intercompari-

Table 2. Mean integrated volume transports as given by the 1/4° (3rd, 4th, and 5th column) and 1/12° (6th, 7th, and 8th column) bathymetry. NN/INT refers to values where only the nearest neighbors (NNs) or interpolated profiles (INTs) were considered. Transport averages are given in Sverdrup (Sv). Negative values indicate southward-directed transport (towards the Indian Ocean).

Strait	Time period average	OBS (1/4°)	GREP	GREP (NN/INT)	OBS (1/12°)	GLORYS12V1	GLORYS12V1 (NN/INT)
Makassar	2004–2017	−9.9	−10.6	−9.7	−9.1	−9.2	−10.8
Lombok	2004–2006	−2.6	−1.5	−1.1	−2.6	−2.5	−2.5
Ombai	2004–2006	−5.3	−3.5	−4.1	−5.1	−4.0	−3.4
Timor	2004–2006	−6.7	−8.9	−9.7	−5.9	−8.7	−9.7

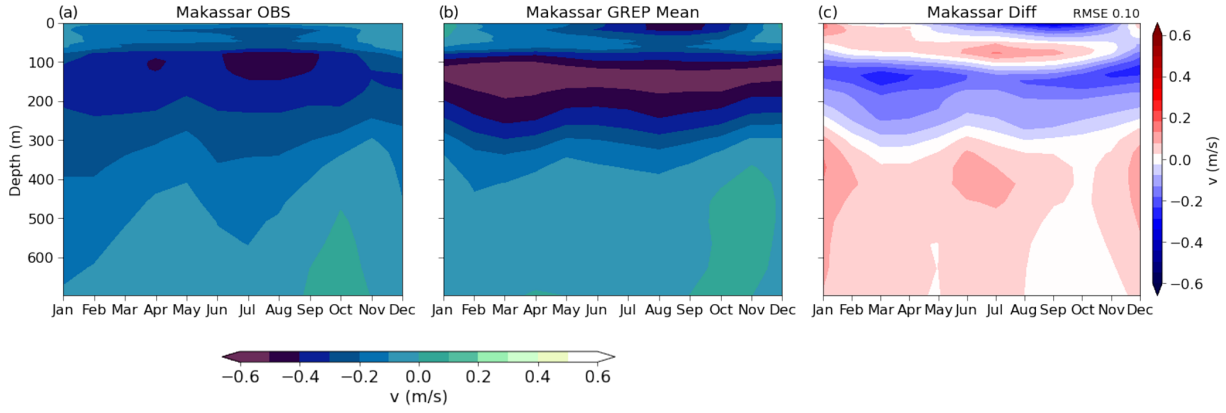

Figure 5. Mean annual cycle of ASVs for the Makassar Strait as given by the 1/4° bathymetry for **(a)** observations and **(b)** the GREP mean. Panel **(c)** refers to their respective differences. RMSE between the observations and the GREP mean is given in the top right corner. Negative values indicate southward transport (toward the Indian Ocean).

son between all considered reanalyses and the observations. The mean annual cycle is most pronounced in the Makassar Strait (Fig. 6a), exhibiting a maximum transport of −12.5 Sv (July in OBS) and −13.6 Sv (August in GREP mean) and a minimum transport of −5.4 Sv (November in OBS) and −6.6 Sv (December in GREP mean). The reduction in transport caused by Kelvin waves can also be assessed in the one-dimensional framework because transport minima in the monsoon transition months represent the intrusion of Kelvin waves. This shows that although the Kelvin wave signal appears suppressed in reanalyses at greater depths (Fig. 5b), it is sufficient to impact the mean annual cycle in all straits (Fig. 6). Furthermore, the annual cycle in the Makassar Strait reveals an apparent time lag of 1 month between the observations and all considered products, which is most pronounced in February to March and July to August. The lag arises both during the INSTANT period (3 years) and in the extended data set (January 2004 to August 2017). To exclude the possibility that the lag occurs just by chance, we assess the significance of the cross-correlation by computing significance barriers. The cross-correlation function peaks at lag 1 at $r(1) = 0.78$ (GREP mean), which is statistically significant on the 95 % level, taking autocorrelation in the individual series into account. This confirms a systematic difference between observations and reanalyses, which will be addressed further below.

The Lombok Strait (Fig. 6b), the Ombai Strait (Fig. 6c), and the Timor Passage (Fig. 6d) do not display such a lag. Also, these straits were only observed during the INSTANT program, meaning that we have a maximum of 3 years' worth of data to determine the mean annual cycle. Representing the ITF's direct outflow passage, the seasonal cycle in the Lombok Strait follows that of the Makassar Strait (Fig. 6a): maximum transport during boreal summer (August in OBS −3.9 Sv; GLORYS12V1 −3.8 Sv) and minimum transport in boreal winter (December in OBS −1.1 Sv; GLORYS12V1 −0.7 Sv). In Lombok the observations display much stronger transports as well as a stronger seasonal cycle compared to the GREP mean (and especially GLORYS2V4, ORAS5, and ORAP6), whereas GLORYS12V1 agrees better with the observations (based on the RMSE of the seasonal cycle curve). This is likely due to its higher resolution and hence its ability to capture seasonal variabilities in narrow straits more accurately.

The annual cycle in the Ombai Strait features distinct minima during the monsoon transition months in April (OBS −3.4 Sv) and October (OBS −3.2 Sv). According to Sprintall et al. (2009), some of the Kelvin wave energy propagating along Sumatra travels further into the Ombai Strait, ex-

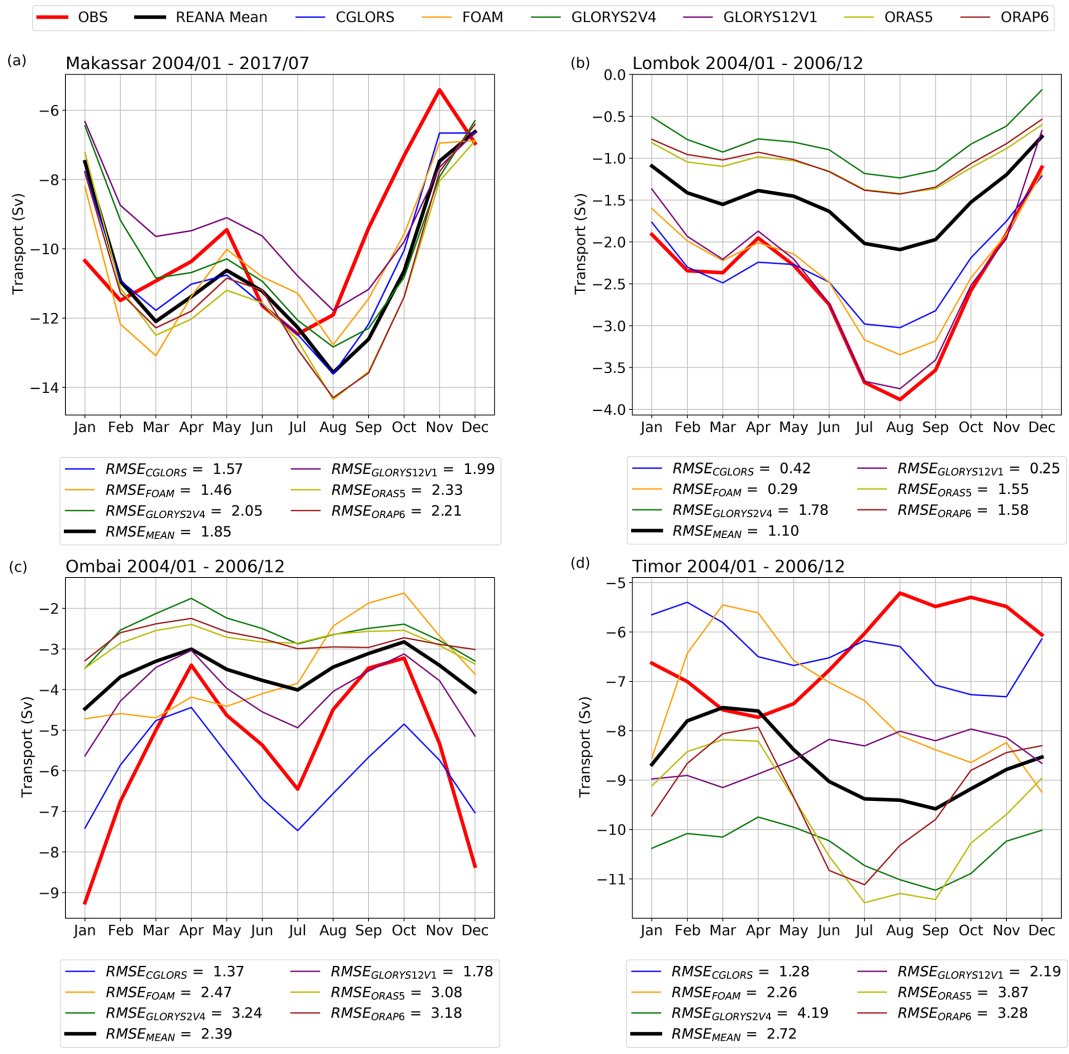

Figure 6. Mean annual cycle of ITF transport in **(a)** the Makassar Strait, **(b)** the Lombok Strait, **(c)** the Ombai Strait, and **(d)** the Timor Passage as represented by observations and reanalyses. Note that Makassar refers to the extended (2004–2017) observation period. Negative values indicate southward-directed transports (towards the Indian Ocean).

plaining the minima in April and October. We find maximum transport during the NW monsoon (January in OBS −9.3 Sv) when both mooring profiles (not shown) display strong subsurface maxima. During the SE monsoon, Ombai transport increases again (July in OBS −6.5 Sv); however, it remains weaker than during the winter months. The GREP mean and GLORYS12V1 converge with the observations during the weak monsoon transition months and increase correctly in the main transport periods of January (GREP mean −4.5 Sv; GLORYS12V1 −5.6 Sv) and July (GREP mean −4.0 Sv; GLORYS12V1 −4.9 Sv). Also, here, reanalysis-based transport strongly underestimates observed transport by up to ∼ 6 Sv in January (especially GLORYS2V4, ORAS5, and ORAP6). Furthermore, the 1/4° products (in contrast to GLORYS12V1) do not capture the asymmetry (positive velocities in the north) in the flow through the Ombai Strait (Fig. A2d–f), further misrepresenting properties in the annual cycle.

The GREP products exhibit a large spread in the Timor Passage, and their ensemble mean strongly deviates from the observations, not only in terms of magnitude but also in seasonal evolution. The observations exhibit minimum and maximum transport during August and September (minimum in August −5.2 Sv) and between March and May (maximum in April −7.9 Sv), respectively. Sprintall et al. (2009) have partly attributed minimum transports to Kelvin wave-induced deep-sea flow reversals that are not captured by the 1/4° products, because they cannot represent flow below ∼ 1200 m due to their bathymetry being too shallow. The GREP mean displays an almost reversed cycle with minimum transport from February to April (minimum in March −7.5 Sv) and maximum transport between July and Septem-

ber (maximum in September −9.6 Sv). The seasonal cycle in GLORYS12V1 is particularly weak, ranging from −7.9 Sv in October to −9.2 Sv in March. However, the correlation between observations and GLORYS12V1 ($r_{\mathrm{GLORYS12V1}} = 0.82$) is by far the highest, keeping in mind the considerable differences in magnitude. Sprintall et al. (2009) suggest that when transport through the Ombai Strait is at a minimum during the monsoon transition months (April to May and October to November), Timor transport increases and vice versa as a result of the well-known Wyrtki Jet (Wyrkti, 1973). Consequently, Kelvin waves associated with the Wyrtki Jet partly control the ITF's annual cycle (Sprintall et al., 2009), and therefore reanalyses need to be able to reproduce them.

From Fig. 6 it is evident that the sum of the outflow passages (Lombok, Ombai, and Timor) is stronger than the inflow from the Makassar Strait. This discrepancy is mostly explained by the flows through the Lifamatola Passage. Measurements (single mooring) were taken in the Lifamatola Passage during INSTANT, but they only cover depths greater than ∼ 400 m. Figure A3a and b show the total transport through the inflow (with Lifamatola contributions added) and outflow passages, respectively. The additional contribution from the Lifamatola Passage shifts the maximum transport during the summer months from August to June in the reanalyses and from July to June in the observations, eliminating the 1-month lag between reanalyses and observations (except GLORYS12V1) we found in Makassar. Note that the reanalysis maximum does not shift when adding only the layer consistent with observations (∼ 400–950 m), suggesting a biased distribution of the reanalyzed flow in this strait as well. Furthermore, reanalysis-based results suggest that a considerable amount of information is lost by only carrying out observations in the Lifamatola Passage without taking into account the whole eastern inflow route. Discrepancies between inflow and outflow transports (Fig. A3) increase around September and last until January, suggesting a more balanced ratio during the summer months. The missing data in the upper 400 m and the fact that the Lifamatola Passage covers only part of the eastern route likely explain those discrepancies.

3.5 Temporal variability

Deseasonalized anomalies of Makassar volume transport between 1993 and 2019 are presented in Fig. 7. Here, positive (negative) anomalies refer to northward-directed (southward-directed) transport anomalies. We find considerable spread between the different reanalysis products, but anomaly correlations with observations are relatively high ($r_{\mathrm{lag}=0}$ ranging between 0.61 (ORAP6) and 0.82 (FOAM)). Temporal standard deviations (SDs) of volume transport exceed 1 Sv in all time series (except ORAS5 0.98 Sv and GLORYS12V1 0.65 Sv), with the highest value in FOAM (1.59 Sv) and moderate deviations in the observations (1.05 Sv), underlining the high variability in the data sets. GLORYS12V1 exhibits weak temporal variability and relatively low correlation with the Nino 3.4 index, which is reflected by the lower SD and a weakly pronounced mean annual cycle (Fig. 6). The signal-to-noise ratio (ratio between SD of the GREP mean and spread of the GREP products Balmaseda et al., 2015) of 1.83 suggests that the products show reasonable agreement in terms of interannual transport variability. Nino 3.4 anomalies in Fig. 7 reveal a strong connection between ITF transport anomalies and ENSO (England and Huang, 2005). The time series show that the ITF is generally out of phase with ENSO, and we find zero-lag correlation coefficients between 0.47 (ORAP6) and 0.8 (OBS). The maximum lagged correlation coefficient reaches 0.86 (OBS) with transport lagging the Nino 3.4 index by 3 months (not shown), suggesting that variabilities in the ITF are a lagged response to ENSO, as also found by England and Huang (2005).

The most prominent signal in the time series marks the period between 2014 and 2016, during which the El Niño event of 2015–2016 occurred, when ITF transport in Makassar is usually reduced due to an eastward-directed anomalous pressure gradient in the Sulawesi Sea (Gordon et al., 2012). The effect of this strong ENSO event is visible in all products, albeit with varying strength. The strong El Niño event is characterized by an extended period of substantial northward-directed anomalies, dominated by transports in CGLORS. This corroborates results by Mayer et al. (2018), who, based on two reanalyses, found that the strongest anomalies of ITF volume transport since 1993 were registered during this period. While observed transports become negative again in mid-2016 with the onset of La Niña, there seems to be an approximately half-year delay in all reanalyses.

We now turn to the cross-sectional view of monthly averaged ASV anomalies (Fig. 8) to address the complex vertical structure of ITF variability in the Makassar Strait. ASV anomalies in Fig. 8 highlight the well-matching structure between observations and the GREP mean, especially in the upper 300 m. Focusing again on the strong El Niño event of 2015–2016, both observations and reanalyses display intensified northward-directed transport anomalies (i.e., weakened flow) in the upper layer (< 300 m) and negative anomalies (i.e., strengthened flow) in the lower layer (> 300 m). Negative anomalies represented by the GREP mean are weaker and extend less far downward than in observations. Thus, the ENSO signal in integrated transports results from compensating anomalies in the upper and lower layer, the balance of which varies across the different products and leads to the considerable spread found in Fig. 7. We will address the effect of such compensating anomalies in detail in Sect. 4. The La Niña event during 2007–2008 marks another distinctive period of negative anomalies reaching down to ∼ 700 m, but again, the GREP mean lacks a signal in deeper layers starting at around 300 m.

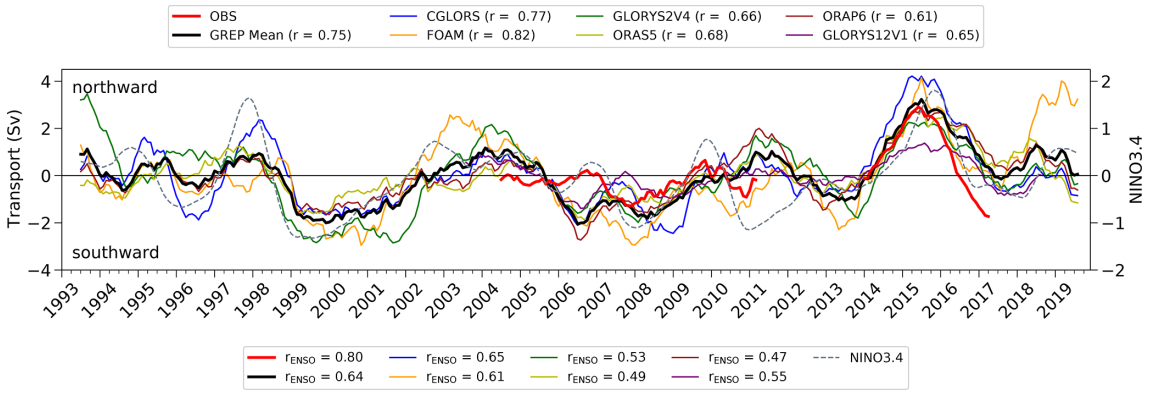

Figure 7. Monthly time series (with 12-month moving average) of total ITF transport anomalies through the Makassar Strait as represented by the observations and the reanalysis products with Nino 3.4 anomalies (Trenberth, 1997). Note the missing observational data between July 2011 and August 2013. Upper legend displays correlation coefficients r between transport anomalies and observation anomalies at lag = 0. Correlation coefficients r_{ENSO} between transport anomalies and the Nino 3.4 anomalies at lag = 0 are given in the lower legend. Negative values indicate southward-directed transports (towards the Indian Ocean).

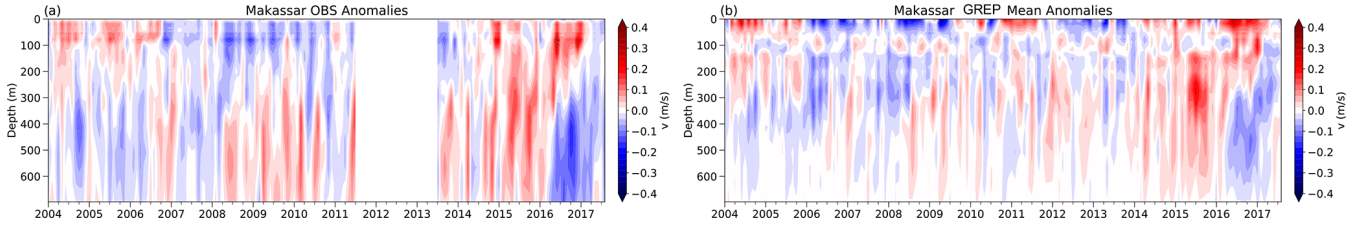

Figure 8. Monthly time series of ASV anomalies in the Makassar Strait as represented by **(a)** the observations and **(b)** the GREP mean. Note the missing observational data between July 2011 and August 2013. Negative values indicate southward-directed velocities (towards the Indian Ocean).

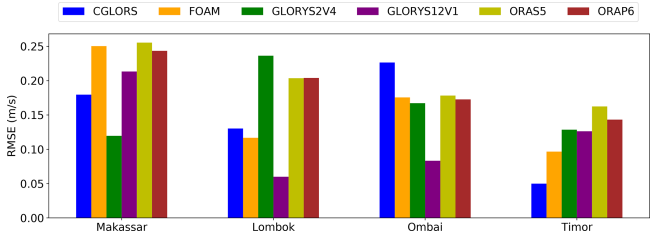

Figure 9. Reanalysis performance: RMSEs of time-averaged vertical profiles of ASV (in $\mathrm{m\,s^{-1}}$) of reanalyses and observations in each strait. Note that Makassar covers the period from 2004–2017, while the other straits have data only from 2004–2006.

3.6 Performance summary metrics

Based on the mean vertical profiles introduced in Fig. 3 and the integrated cross-sections in Fig. 4, we now present a more systematic evaluation of all considered reanalyses in each strait. The evaluation rests on different applications of the root mean square error (RMSE) in reference to the observations and the bias of reanalyses. While the observations are certainly not free of errors, we regard them as truth here. Any deviation from observations is considered an error.

Figure 9 shows the performance of each product in terms of RMSEs of time-averaged vertical profiles (NN/INT) of ASV in all straits. Results depend on the reanalyses' capabilities to accurately represent velocity profiles at the mooring sites. This, in turn, depends on the representation of asymmetries in the flow. There is considerable spread between the GREP products in the Makassar Strait, with the RMSE of FOAM, ORAS5, and ORAP6 being almost twice as large as that of GLORYS2V4 (Fig. 3). The successor of ORAS5, ORAP6, shows a slight improvement. Although GLORYS12V1 is able to resolve grid points that are much more closely located to the mooring sites, its performance is surprisingly mediocre in Makassar. GLORYS12V1, the higher-resolving version of GLORYS2V4, exhibits a larger RMSE than GLORYS2V4. This can partly be attributed to the greatly overestimated flow in the surface layer in GLORYS12V1 (Fig. 3). We note that velocities are generally strongest in the Makassar Strait, and hence the comparatively large RMSEs in this strait do not necessarily mean larger relative errors.

In the Lombok Strait and the Timor Passage, spread across the GREP products is also large, while there is a better agreement in the Ombai Strait (within the reanalyses). GLO-

RYS12V1 has an advantage over the 1/4° products particularly in the narrow Lombok and Ombai straits. In the Lombok Strait, the stronger surface layer currents, especially towards the west, are accurately represented by GLORYS12V1, unlike the GREP products. Also, in the Ombai Strait, opposite transport orientation between the north and south in the upper ~ 200 m is only represented in GLORYS12V1 (Fig. A1). There are four mooring sites in the Timor Passage and hence four comparisons to consider (Fig. A1). Discrepancies between observations and CGLORS are comparatively small in each layer at all sites, which explains the good performance of CGLORS. Most 1/4° products yield better agreement away from the coast, whereas GLORYS12V1 seems to increase its skill towards the mainland (Timor; Fig. A1).

Figure 10 summarizes the performance of all reanalysis products based on monthly time series of integrated volume transport in each strait. Taking into account all horizontal grid points, these results reveal additional strengths and weaknesses of the products in terms of performance. In the Makassar Strait, the spread between the GREP products decreases considerably compared to Fig. 9. The performances of ORAS5 and ORAP6 are dominated by their overestimated velocities as represented by the bias (Fig. 10a) and the mean seasonal cycle (Fig. 10b). The bias points towards a moderate overestimation in all products, which is particularly small in the GLORYS products. By removing the seasonal pattern (Fig. 10c), the spread between the products barely changes. However, ORAS5 and ORAP6 no longer perform the worst, and GLORYS12V1 displays its advantages.

Figure 6b highlights the considerable underestimation of transports in GLORYS2V4, ORAS5, and ORAP6 in the Lombok Strait. Accordingly, these products exhibit a strong negative bias (Fig. 10a), and Fig. 10b confirms earlier results with the highest RMSE in GLORYS2V4. Two horizontal grid points are clearly not enough to cover transport through Lombok. Still, CGLORS and FOAM exhibit good agreement with observations. However, this is not because they represent the asymmetry in the flow correctly but because they provide generally high transport values (Fig. 6b), decreasing the RMSEs between observations and reanalyses. Thus, GLORYS12V1 (representing Lombok with four grid points) represents the spatial distribution of ASVs (not shown) correctly, likely explaining its low bias.

The GREP products also cover the Ombai Strait with only two grid points, but the observed and reanalyzed mean transport doubles in magnitude (Table 2). Also here, the three reanalyses GLORYS2V4, ORAS5, and ORAP6 display considerable shortcomings in terms of the mean and seasonal variations (Fig. 6a and Fig. 6b). CGLORS shows good performance in Ombai (even outperforming GLORYS12V1). It exhibits the strongest mean flow and the most accurate representation of the annual cycle.

The Timor Passage displays high bias-corrected RMSEs, which is already evident from the inconsistencies we addressed in Fig. 6d. We find a similar ranking of the products as in Lombok and Ombai with a considerable discrepancy between the worst-performing (GLORYS2V4) and the best-performing product (CGLORS). GLORYS2V4 has a strong positive ASV bias towards the surface (Fig. A1), which also appears in GLORYS12V1 (Fig. A1) but is reduced towards the south due to additional grid points. Figure 9 reveals the superior performance of CGLORS, which is reflected by the bias and the RMSE of the mean seasonal cycle likely caused by the non-overestimation of the flow in the upper ~ 200 m (Fig. A1; followed by FOAM).

4 Two-layer regime

Dividing the water column in the Makassar Strait into two layers, the upper layer (< 300 m) and lower layer (> 300 m) (Gordon et al., 2019; Pujiana et al., 2019), reveals interesting properties of the ITF. Figure 11 shows transport anomalies in the upper and lower layers as represented by the observations (Fig. 11a), the GREP mean (Fig. 11b), and GLORYS12V1 (Fig. 11c). There is a clear anti-correlation between upper and lower layers, with correlations of $r_{\text{lag}=-1} = -0.37$ (p value $= 2.3 \times 10^{-3}$), $r_{\text{lag}=-1} = -0.30$ (p value $= 1.1 \times 10^{-2}$), and $r_{\text{lag}=-1} = -0.45$ (p value $= 7.7 \times 10^{-5}$), respectively. For the calculation of the respective p values, we consider the autocorrelation of the time series and estimated the effective sample size n_{eff} based on equation B12 in Oort and Yienger (1996). By comparing Figs. 7 and 11, we find similar behavior of full-depth integrated transport anomalies and upper-layer anomalies ($r_{\text{OBS}} = 0.49$), indicating that transport anomalies within the upper 300 m dominate the sign of the integrated anomaly. This behavior is reproduced by the GREP mean ($r_{\text{RMEAN}} = 0.89$) and GLORYS12V1 ($r_{\text{GLORYS12V1}} = 0.85$). Observations display almost equally strong upper- and lower-layer anomalies, with even a dominant lower-layer anomaly in October 2016, after the strong El Niño event. The GREP mean and GLORYS12V1 exhibit comparatively weak lower-layer anomalies ranging between $[-1.6; 1.6]$ Sv and $[-1.4; 0.9]$ Sv, respectively, which is consistent with their weak mean flow at depth (Fig. 3).

Monthly transport anomalies and monthly sea level gradient anomalies are negatively correlated in the upper layer ($r_{\text{OBS}} = -0.61$, $r_{\text{RMEAN}} = -0.83$, and $r_{\text{GLORYS12V1}} = -0.81$). Accordingly, higher mean sea level anomalies in the Pacific (Indian Ocean) correspond to southward-directed (northward-directed) transport anomalies, which is consistent with the large-scale sea level gradient. The correlation reverses in the lower layer, indicating that the relation between transport and sea level difference anomalies no longer follows the force of the sea level gradient. Therefore, we conclude that the upper layer is regulated by the sea level gradient, while baroclinic effects dominate in lower layers.

To investigate the apparent two-layer behavior further, Fig. 12 presents diagnostics targeted at a better understanding of depth-dependent relationships between oceanic

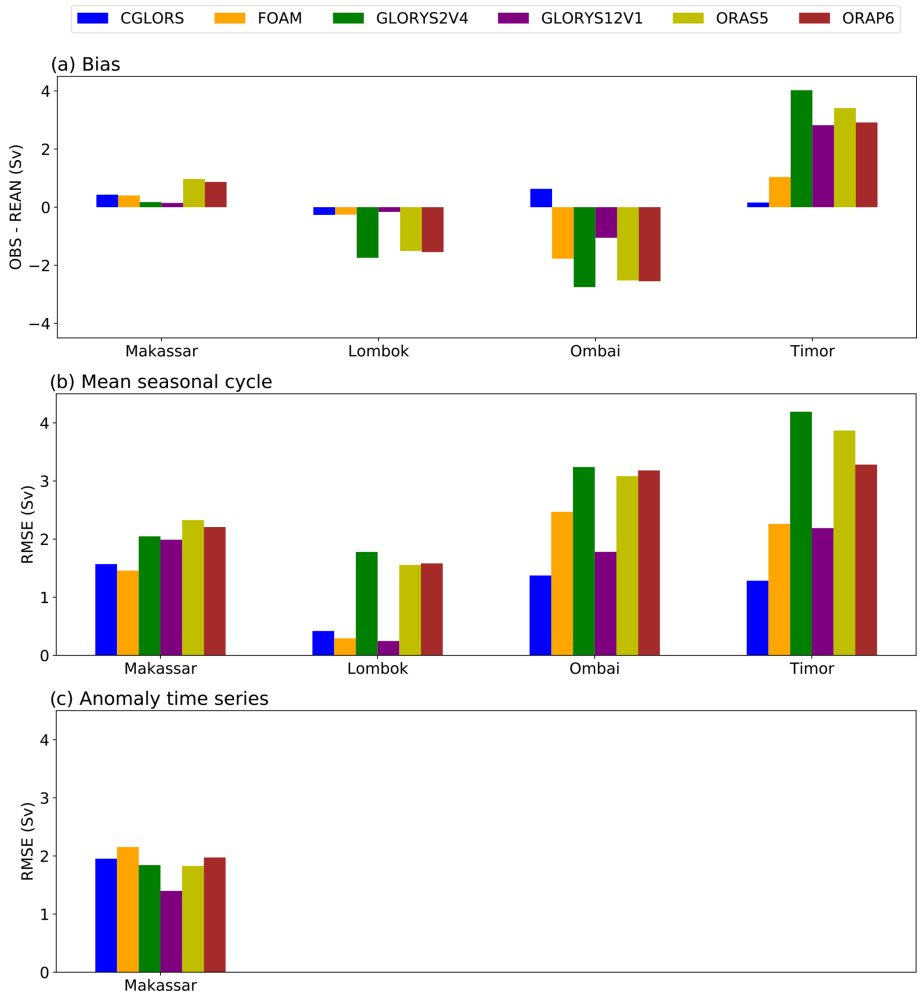

Figure 10. Reanalysis performance: **(a)** biases (in Sv) in reanalyses based on monthly time series of ITF transport in each strait. RMSEs of **(b)** mean seasonal cycles of ITF transport (in Sv) and **(c)** monthly time series of ITF transport (in Sv) anomalies and observations in the Makassar Strait (outflow straits cover only 3 years and are therefore not considered). Note that Makassar covers the period from 2004–2017.

flow and pressure gradients. First, Fig. 12a shows a depth-dependent cross-correlation of ASVs through the Makassar Strait from observations and the GREP mean. We find maximum positive correlations at a lag of 1 month (from 70–200 m and 450–500 m), indicating that the GREP mean leads transport by about 1 month (Fig. 6a). A partition of the mean seasonal cycle into the upper (< 300 m) and the lower (> 300 m) layer reveals that the lag is more pronounced in the lower layer, where reanalyses exhibit weak current velocities. The maximum correlation at lag $= 1$ is also present when performing a similar diagnostic only on the annual cycle of transports (Fig. A4a), which is consistent with the results shown in Fig. 6a. We amplify its effect by considering a 10-year time series consisting only of the mean seasonal cycle.

Next, we study the relationship between the interocean pressure gradient and ASV anomalies in Makassar. The regions used for computation of the pressure gradient were chosen based on spatial correlation patterns between sea level anomalies (SLAs) and ASV anomalies (boxes in Fig. 1). Note that the chosen regions are similar to those used in Mayer et al. (2018) and Pujiana et al. (2019). Cross-correlations between pressure gradient anomalies at $z = 0$, which are proportional to the SLA gradient, and ASV anomalies for the GREP mean and observations are assessed in Fig. 12b and e, respectively. The results for both data types display similar properties: while maximum negative correlations ($r_{\mathrm{GREP}} = -0.81$, $r_{\mathrm{OBS}} = -0.69$) dominate the upper layer around lag 0, positive correlations govern the lower layer and become most notable towards lag -1. This confirms that transports driven by sea level gradients are an upper-layer phenomenon, and the lower layer is detached from the geostrophic flow near the surface. Covariances in Fig. 12d complement these results and highlight that the covariance between observations and reanalyses is still considerable at depths of ~ 300–500 m.

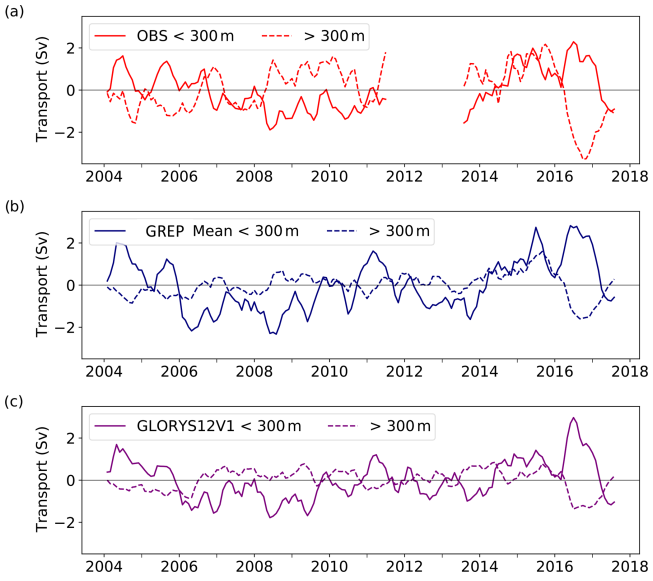

Figure 11. Monthly time series of ITF transport anomalies through the Makassar Strait in the upper (continuous lines) and lower (dashed lines) layers as represented by **(a)** observations, **(b)** GREP mean, and **(c)** GLORYS12V1. Considered time series cover the period between 2004 and 2017. Negative values indicate southward-directed transports (towards the Indian Ocean).

Figure 12c and f show cross-correlations between the pressure gradient as a function of depth (based on reanalysis data) and ASVs from reanalyses and observations, respectively. The continuous negative correlations highlight that although transport anomalies in the upper and lower layer oppose each other, they are still regulated by the vertically varying pressure gradient. ASVs and pressure gradients both decrease with depth, and accordingly, correlations decrease with depth (more so in Fig. 12c). Both observations and the GREP mean exhibit maximum correlation with the gradient at lag 0, indicating that the differences in Figs. 12a and A4a could arise from an "ageostrophic" part of the flow. Such processes have been attributed to baroclinic Kelvin waves that originate in the equatorial Indian Ocean and dictate the two-layer system of ITF transport anomalies (Pujiana et al., 2019). Drushka et al. (2010) traced the pathways of Kelvin waves from their point of origin (equatorial Indian Ocean) into the ITF region using altimetric SLA data and found that Kelvin waves are not linked to the large-scale sea level gradient but rather local anomalies, explaining the disappearing connection between sea level gradient anomalies and ASV anomalies at greater depths.

We note that correlations in the lower layer are higher for the observations. To assess the robustness of the reanalysis-based pressure gradient, we attempted to obtain an observation-based estimate of the pressure gradient using subsurface ocean temperature and salinity profiles from the EN4 data sets (UK Met Office Good et al., 2013), but insufficient data coverage did not allow us to obtain robust results. Regarding the weak correlation around 100 m in Fig. 12b and c, we did verify that this is not due to cross-passage extrapolation over the shelf.

5 Conclusions

In this paper, we compared observations of oceanic flow in the ITF region from instruments installed on moorings with ocean reanalysis data. Firstly, the skill and limit of different ocean reanalysis products within the Makassar Strait, the Lombok Strait, the Ombai Strait, and the Timor Passage were assessed. This required careful preprocessing of both data types. Results are sensitive to how the bathymetry was used for the cross-passage extrapolation of along-strait velocities (ASVs) and the use of boundary conditions, which indicates considerable uncertainties associated with transport calculations based on sparse mooring-based measurements.

Intercomparisons between observations and reanalyses revealed generally positive (overestimation) and negative (underestimation) biases of transport in broad and narrow straits, respectively. GLORYS12V1 exhibited advantages in Makassar and the Lombok Strait, suggesting that the higher-resolving reanalysis (more horizontal grid points) is capable of improving representations in both broader and narrow straits. In terms of representing the annual mean bias and the mean seasonal cycle (Fig. 10a and b, respectively), CGLORS shows generally high skill, especially in the Ombai Strait and the Timor Passage (even outperforming the higher-resolving GLORYS12V1). Based on our diagnostics, we found that all reanalyses exhibit currents that are too weak at greater depths. Furthermore, the $1/4°$ reanalysis products struggled with locating the core of the flow in the cross-sections, misrepresenting frequently occurring spatial asymmetries in the flow through the passages. As a result of the higher resolution of GLORYS12V1, the representation of such asymmetries did improve. This was also reflected in the long-term mean integrated transports, where GLORYS12V1 agrees much better with observations than the other GREP products in all straits except the Timor Passage. Comparisons between observations and reanalysis data taken only at the mooring locations showed that not considering all grid points can improve the agreement between observational and reanalysis-based transport values in some straits (Makassar and Ombai), possibly indicating observational undersampling in these straits or biased structures of the flow (in reanalyses), but can lead to strong over- and underestimation in other straits (Lombok and Timor) as a result of mislocated maxima in the passages. Given the biased structure of the flow in some straits, the usefulness of reanalyses to choose suitable mooring sites is limited. Despite the mean velocity biases evident in most reanalyses, the observations were within the range of the GREP in most cases. This study shows that the complex structure of the ITF region remains

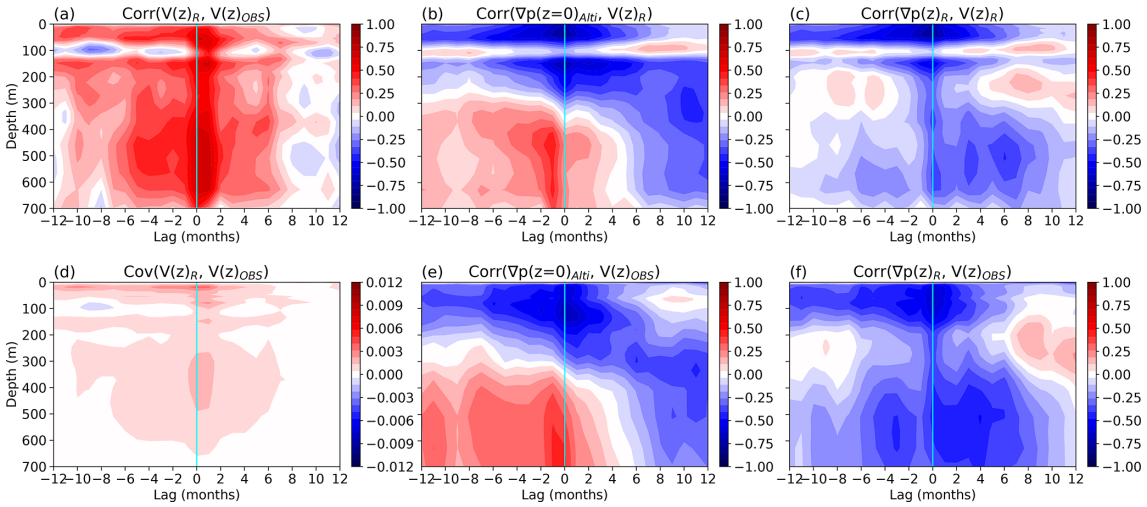

Figure 12. Depth-dependent lead–lag **(a)** correlations and **(d)** covariances between observed $V(z)_{\mathrm{OBS}}$ and GREP mean-based $V(z)_{\mathrm{R}}$ ASV anomalies in Makassar. Depth-dependent lead–lag correlations between monthly time series of **(b)** GREP mean-based sea level gradient anomalies $\nabla \mathrm{p(z=0)}_{\mathrm{Alti}}$ and ASV anomalies $V(z)_{\mathrm{R}}$ and **(e)** observed ASV anomalies $V(z)_{\mathrm{OBS}}$ in Makassar. Depth-dependent lead–lag correlation between monthly time series of GREP mean-based pressure gradient anomalies $\nabla p(z)_{\mathrm{R}}$ and ASV anomalies **(c)** $V(z)_{\mathrm{R}}$ and **(f)** $V(z)_{\mathrm{OBS}}$ in Makassar. Sea level gradients and pressure gradient anomalies refer to the ITF's entrance and exit region as indicated in Fig. 1. Considered time series cover the period between 2004 and 2017.

a challenging area for reanalyses, but higher-resolving products (GLORYS12V1) provide a promising outlook.

In the second part of the paper, we explored the annual cycle and vertical structure of the flow and involved processes in more detail. The mean annual cycle of ITF transport, which is strongly influenced by Kelvin waves in all passages, highlighted the importance of representing Kelvin wave activity in the reanalyses. Reanalyses generally exhibit flow that is too weak at greater depths and weaker Kelvin wave activity in deeper layers compared to expectations from observational studies like Sprintall et al. (2009). We also addressed the apparent time lag of 1 month in the mean annual cycle between the observations and all considered reanalysis products in the Makassar Strait. The lag in the inflow was largely removed when taking into account additional measurements/reanalysis data from the Lifamatola Passage, which indicates that the seasonal distribution of flow between Makassar and the Lifamatola Passage is different in reanalyses compared to observations. However, it must be noted that observational coverage in the Lifamatola Passage is suboptimal.

For a better understanding of the vertical structure of the flow, we investigated the relationship between the vertically varying horizontal pressure gradient and ASV anomalies in Makassar. We found that different mechanisms are responsible for driving the upper-layer (< 300 m) and lower-layer (> 300 m) flow: the sea level gradient regulates transport anomalies in the upper layer, and baroclinic effects dominate in lower layers. Their origins are the subject of current research and have been mostly attributed to baroclinic Kelvin waves that originate in the equatorial Indian Ocean (Pujiana et al., 2019). A more accurate representation of deep-layer ASVs in reanalyses is necessary to investigate the two-layer mechanism in detail and the corresponding impact of Kelvin waves on the ITF. We also found that the net ITF response to ENSO (typically weaker during El Niño and stronger during La Niña) is the result of dominant signals in the upper layer and counteracting anomalies in the lower layer. The balance of these opposing signals differs between observations and reanalyses (and within reanalyses). Accurate representation of these processes in reanalyses is clearly needed because of their relevance for climate monitoring. However, long-term observations, especially in the outflow passages, are also necessary to improve the observational sampling of interannual and longer-term variations of the ITF.

Appendix A

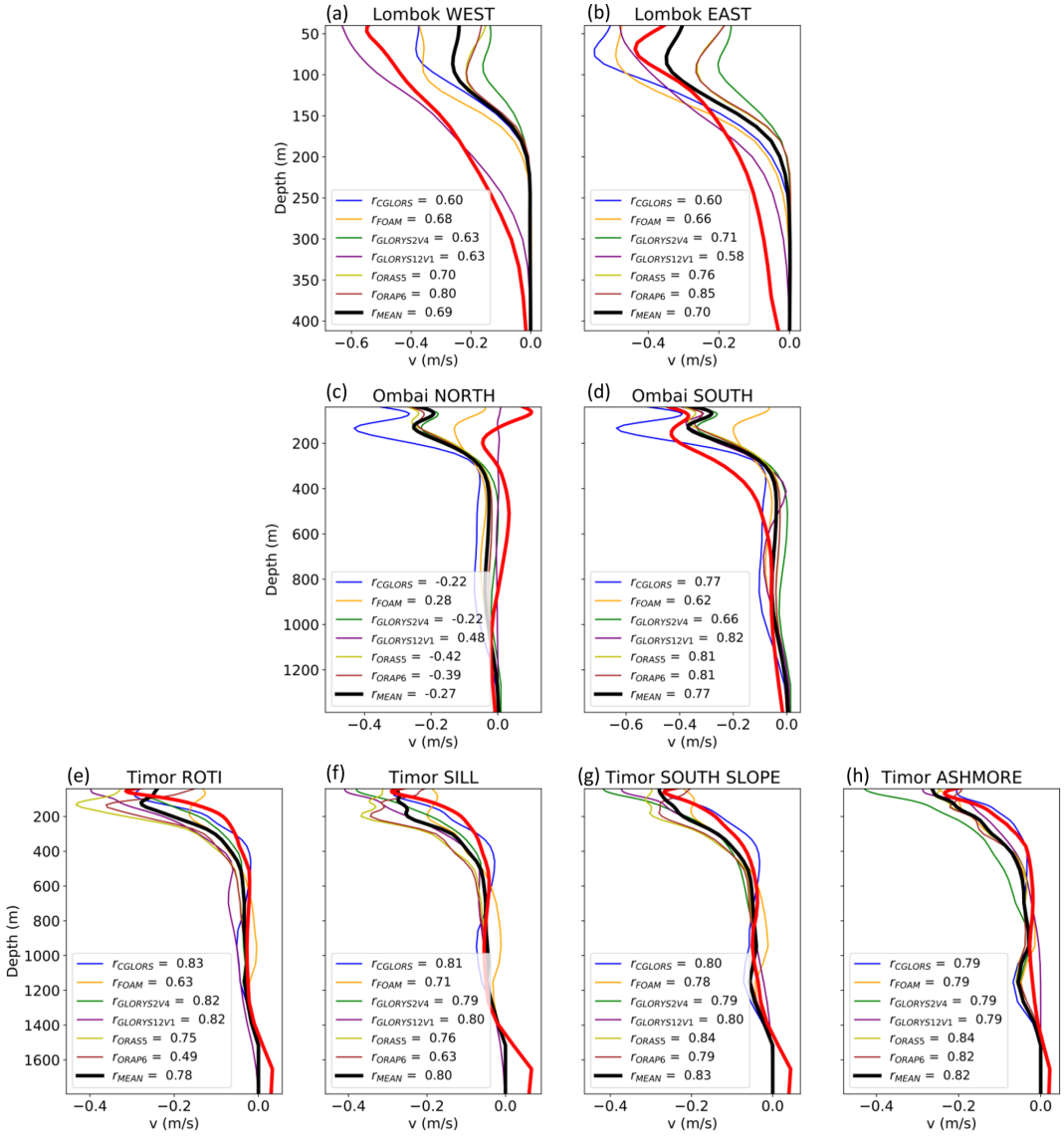

Figure A1. Mean ASV profiles for **(a–b)** the Lombok Strait, **(c–d)** the Ombai Strait, and **(e–h)** the Timor Passage. Purely spatial Pearson correlation coefficients between observation-based and reanalysis-based temporally averaged ASV profiles across depth are given in the boxes on the lower left. Negative values indicate southward-directed velocities (towards the Indian Ocean).

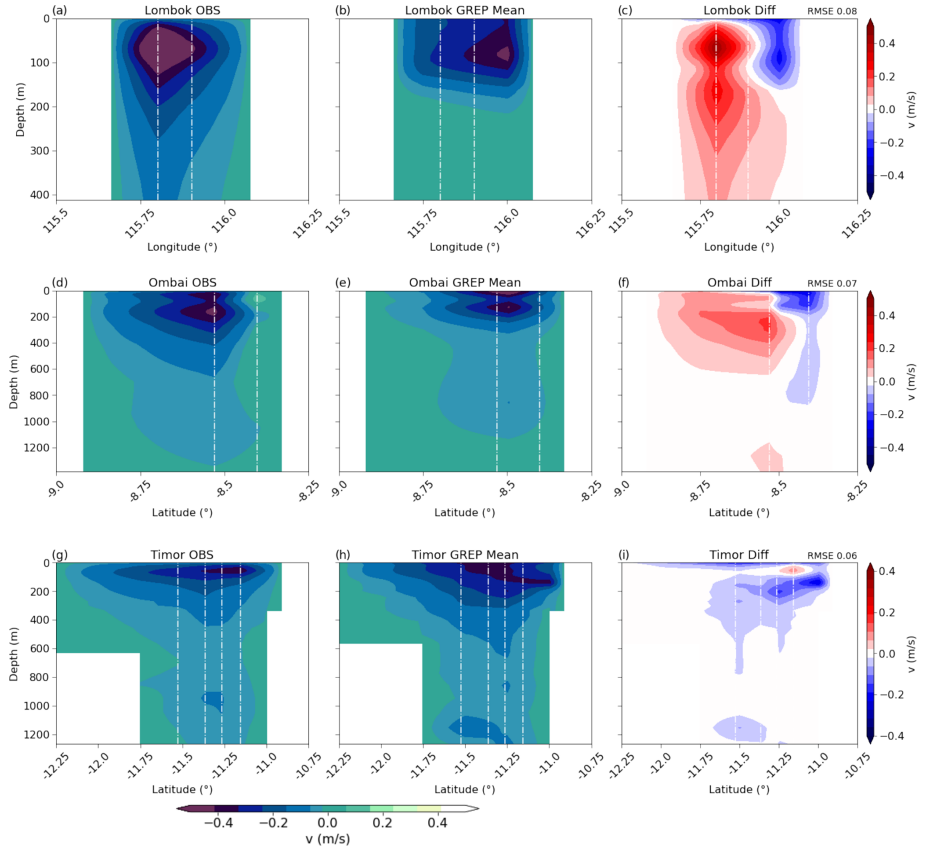

Figure A2. Mean ASV cross-sections for **(a–c)** the Lombok Strait, **(d–f)** the Ombai Strait, and **(g–i)** the Timor Passage as given by the observations (left) and the GREP mean (middle). The far right column corresponds to the respective differences between observations and GREP mean with the RMSE given in the top right corner. White dash–dot lines represent mooring locations. Negative values indicate southward-directed velocities (towards the Indian Ocean).

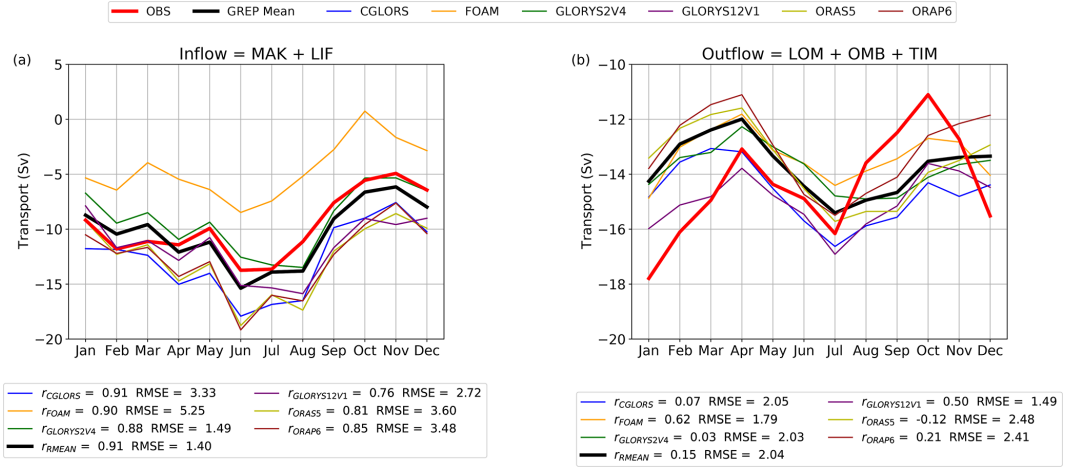

Figure A3. Mean annual cycles of ITF transport through **(a)** the inflow passages (= the Makassar Strait + the Lifamatola Passage) and **(b)** the outflow passages (= the Lombok Strait + the Ombai Strait + the Timor Passage) as represented by observations and reanalyses. Observations in the Lifamatola Passage are only available below 400 m. Subjacent boxes display corresponding Pearson correlation coefficients r and RMSEs. Note that all annual cycles refer to the INSTANT period (January 2004–December 2006). Negative values indicate southward-directed transports (towards the Indian Ocean).

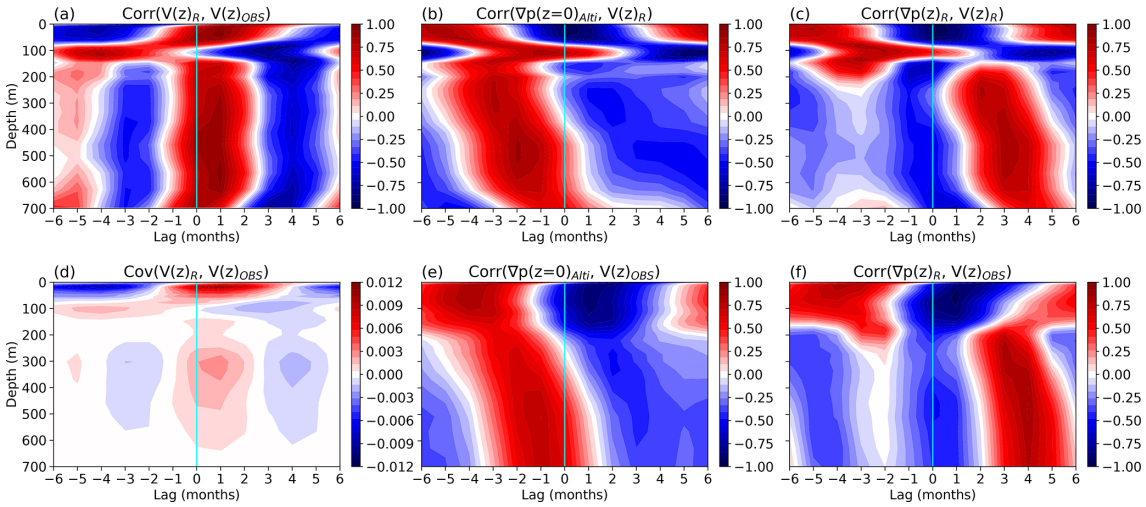

Figure A4. Analogous to Fig. 12 except the observed and reanalysis-based monthly time series are replaced by 10-year time series consisting only of the mean annual cycle. Sea level gradients and pressure gradients refer to the ITF's entrance and exit region. Considered time series cover the period between 2004 and 2017. Red (blue) values indicate positive (negative) correlations.

Data availability. The INSTANT data sets can be accessed online (http://www.marine.csiro.au/~cow074/instantdata.htm, Cowley, 2011). The employed ocean reanalysis data can be obtained from the Copernicus Marine Data Store (https://data.marine.copernicus.eu/products, Copernicus Marine Service, 2019). The Nino 3.4 index is a product of the National Oceanic and Atmospheric Administration (NOAA) Physical Sciences Laboratory (PSL) using the HadISST1 data set (https://psl.noaa.gov/gcos_wgsp/Timeseries/Data/nino34.long.data, NOAA Physical Sciences Laboratory, 2003).

Author contributions. MF and MM conceptualized the study. All co-authors were involved with data preparation and analysis as well as interpretation of results. MF prepared the manuscript with contributions from all co-authors.

Competing interests. The contact author has declared that none of the authors has any competing interests.

Disclaimer. Publisher's note: Copernicus Publications remains neutral with regard to jurisdictional claims in published maps and institutional affiliations.

Acknowledgements. We sincerely thank Rebecca Cowley from the Commonwealth Scientific and Industrial Research Organisation (CSIRO) for clarifying any issues with the INSTANT data set and for cross-checking first attempts. We would also like to acknowledge the help of Janet Sprintall from the Scripps Institution of Oceanography at the University of California San Diego for reviewing our preprocessing methods and providing additional material. We thank Michael McPhaden from the National Oceanic and Atmospheric Administration (NOAA) for sharing his expertise and providing useful feedback on our diagnostics. We would like to thank the two anonymous reviewers, whose comments helped to improve the manuscript. Open-access funding was provided by University of Vienna. Magdalena Fritz and Michael Mayer received funding from CMEMS 21003-COP-GLORAN Lot 7. Michael Mayer and Susanna Winkelbauer received additional funding from the Austrian Science Fund project P33177.

Financial support. This research has been supported by the Austrian Science Fund (grant no. P33177) and grant CMEMS 21003-COP-GLORAN Lot 7.

Review statement. This paper was edited by Erik van Sebille and reviewed by two anonymous referees.

References

Arakawa, A. and Lamb, V.: Computational Design of the Basic Dynamical Processes of the UCLA General Circulation Model, Method. Comput. Phys., 17, 173–265, https://doi.org/10.1016/B978-0-12-460817-7.50009-4, 1977.

Argo: Argo float data and metadata from Global Data Assembly Centre (Argo GDAC), SEANOE [data set], https://doi.org/10.17882/42182, 2000.

Asbjørnsen, H., Arthun, M., Skagseth, Ø., and Eldevik, T.: Mechanisms of Ocean Heat Anomalies in the Norwegian Sea, Clim. Dynam., 124, 2908–2923, https://doi.org/10.1029/2018JC014649, 2019.

Balmaseda, M. A., Trenberth, K. E., and Källén, E.: Distinctive climate signals in reanalysis of global ocean heat content, Geophys. Res. Lett., 40, 1754–1759, https://doi.org/10.1002/grl.50382, 2013.

Balmaseda, M. A., Hernandez, F., Storto, A., Palmer, M. D., Alves, O., Shi, L., Smith, G. C., Toyoda, T., Valdivieso, M., Barnier, B., Behringer, D., Boyer, T., Chang, Y.-S., Chepurin, G. A., Ferry, N., Forget, G., Fujii, Y., Good, S., Guinehut, S., Haines, K., Ishikawa, Y., Keeley, S., Köhl, A., Lee, T., Martin, M. J., Masina, S., Masuda, S., Meyssignac, B., Mogensen, K., Parent, L., Peterson, K. A., Tang, Y. M., Yin, Y., Vernieres, G., Wang, X., Waters, J., Wedd, R., Wang, O., Xue, Y., Chevallier, M., Lemieux, J.-F., Dupont, F., Kuragano, T., Kamachi, M., Awaji, T., Caltabiano, A., Wilmer-Becker, K., and Gaillard, F.: The Ocean Reanalyses Intercomparison Project (ORA-IP), The Ocean Reanalyses Intercomparison Project (ORA-IP), 8, 80–97, https://doi.org/10.1080/1755876X.2015.1022329, 2015.

Boy, R.: Lombok Strait: An Indonesian Throughflow Passage, Oseana, 2, 33–40, 1995.

Cabanes, C., Grouazel, A., von Schuckmann, K., Hamon, M., Turpin, V., Coatanoan, C., Paris, F., Guinehut, S., Boone, C., Ferry, N., de Boyer Montégut, C., Carval, T., Reverdin, G., Pouliquen, S., and Le Traon, P.-Y.: The CORA dataset: validation and diagnostics of in-situ ocean temperature and salinity measurements, Ocean Sci., 9, 1–18, https://doi.org/10.5194/os-9-1-2013, 2013.

Clarke, A. J. and Liu, X.: Observations and dynamics of semiannual and annual sea levels near the eastern equatorial Indian Ocean boundary, J. Phys. Oceanogr., 23, 386–399, https://doi.org/10.1175/1520-0485(1993)023<0386:OADOSA>2.0.CO;2, 1993.

Clarke, A. J. and Liu, X.: Interannual sea level in the northern and eastern Indian Ocean, J. Phys. Oceanogr., 24, 1224–1235, https://doi.org/10.1175/1520-0485(1994)024<1224:ISLITN>2.0.CO;2, 1994.

Copernicus Marine Service (CMEMS): Global Ocean Physics Reanalysis, CMEMS [data set], https://data.marine.copernicus.eu/products (last access: 7 August 2023), 2019.

Cowley, R., Heaney, B., Wijffels, S., Pender, L., Sprintall, J., Kawamoto, S., and Molcard, R.: INSTANT Sunda Data Report Description and Quality Control, CSIRO Marine and Atmospheric Research, http://www.marine.csiro.au/~cow074/INSTANTdataQC_v4.pdf (last access: 8 August 2023), 2009.

Cresswell, G.: Coastal currents of northern Papua New Guinea, and the Sepik River outflow, Mar. Freshwater Res., 51, 553–564, https://doi.org/10.1071/MF99135, 2000.

Cowley, R.: INSTANT, CSIRO Marine Research [data set], http://www.marine.csiro.au/~cow074/instantdata.htm (last access: 7 August 2023), 2011.

Dee, D. P., Uppala, S. M., Simmons, A. J., Berrisford, P., Poli, P., Kobayashi, S., Andrae, U., Balmaseda, M. A., Balsamo, G., Bauer, P., Bechtold, P., Beljaars, A. C. M., van de Berg, L., Bidlot, J., Bormann, N., Delsol, C., Dragani, R., Fuentes, M., Geer, A., and Vitart, F.: The ERA-Interim reanalysis: configuration and performance of the data assimilation system, Q. J. Roy. Meteor. Soc., 137, 553–597, https://doi.org/10.1002/qj.828, 2011.

Desportes, C., Drévillon, M., Drillet, Y., Garric, G., Parent, L., Régnier, C., Masina, S., Storto, A., Petterson, D., Wood, R., Balmaseda, M., and Zuo, H.: GREP: Evaluation of the Copernicus Marine Service Global Reanalysis Ensemble Product: deriving uncertainty estimates for 3D T and S variability in the ocean, Geophys. Res. Abstr., EGU2017-16232, EGU General Assembly 2017, Vienna, Austria, 2017.

Dobricic, S. and Pinardi, N.: An oceanographic three-dimensional variational data assimilation scheme, Ocean Model., 22, 89–105, https://doi.org/10.1016/j.ocemod.2008.01.004, 2008.

Drushka, K., Sprintall, J., Gille, S. T., and Brodjonegoro, I.: Vertical structure of Kelvin waves in the Indonesian Throughflow exit passages, J. Phys. Oceanogr., 40, 1965–1987, https://doi.org/10.1175/2010JPO4380.1, 2010.

Ekman, V. W.: On the Influence of the Earth's Rotation on Ocean-Currents, Arkiv For Matematik, Astronimi och Fysik, 2, no. 11, 1905.

England, M. H. and Huang, F.: On the Interannual Variability of the Indonesian Throughflow and Its Linkage with ENSO, J. Clim., 18, 1435–1444, https://doi.org/10.1175/JCLI3322.1, 2005.

Garric, G. and Parent, L.: Quality Information Document For Global Ocean Reanalysis Products, https://catalogue.marine.copernicus.eu/documents/QUID/CMEMS-GLO-QUID-001-025.pdf (last access: 28 May 2022), 2017.

Godfrey, J. S.: The effect of the Indonesian Throughflow on ocean circulation and heat exchange with the atmosphere: A review, J. Geophys. Res., 101, 12217–12237, https://doi.org/10.1029/95JC03860, 1996.

Good, S. A., Martin, M. J., and Rayner, N. A.: EN4: quality controlled ocean temperature and salinity profiles and monthly objective analyses with uncertainty estimates, J. Geophys. Res.-Ocean., 118, 6704–6716, https://doi.org/10.1002/2013JC009067, 2013.

Gordon, A. L.: Oceanography of the Indonesian Seas and Their Throughflow, Oceanography, 18, 14–27, https://doi.org/10.5670/oceanog.2005.01, 2005.

Gordon, A. L., Susanto, R. D., Ffield, A., Huber, B. A., Pranowo, W., and Wirasantosa, S.: Makassar Strait throughflow, 2004 to 2006, Geophys. Res. Lett., https://doi.org/10.1029/2008GL036372, 2008.

Gordon, A. L., Huber, B. A., Metzger, J. E., Susanto, D. R., Hurlburt, H. E., and Adi, R. T.: South China Sea throughflow impact on the Indonesian throughflow, Geophys. Res. Lette., 39, L11602, https://doi.org/10.1029/2012GL052021, 2012.

Gordon, A. L., Napitu, A., Huber, B. A., Gruenburg, L. K., Pujiana, K., and Agustiadi, T.: Makassar Strait Throughflow Seasonal and Interannual Variability: An Overview, J. Geophys. Res.-Ocean., 124, 3724–3736, https://doi.org/10.1029/2018JC014502, 2019.

Hersbach, H., Bell, B., Berrisford, P., Hirahara, S., Horányi, A., Muñoz Sabater, J., Nicolas, J., Peubey, C., Radu, R., Schepers, D., Simmons, A., Soci, C., Abdalla, S., Abellan, X., Balsamo, G., Bechtold, P., Biavati, G., Bidlot, J., Bonavita, M., and Thépaut, J. N.: The ERA5 global reanalysis, Q. J. Roy. Meteor. Soc., 146, 1999–2049, https://doi.org/10.1002/qj.3803, 2020.

Large, W. G. and Yeager, S.: Diurnal to decadal global forcing for ocean and sea-ice models: the data sets and flux climatologies, NCAR Technical Note, NCAR/TN-460+STR, CGD Division of the National Center for Atmospheric Research, https://doi.org/10.5065/D6KK98Q6, 2004.

Lellouche, J.-M., Greiner, E., Le Galloudec, O., Garric, G., Regnier, C., Drevillon, M., Benkiran, M., Testut, C.-E., Bourdalle-Badie, R., Gasparin, F., Hernandez, O., Levier, B., Drillet, Y., Remy, E., and Le Traon, P.-Y.: Recent updates to the Copernicus Marine Service global ocean monitoring and forecasting real-time 1/12° high-resolution system, Ocean Sci., 14, 1093–1126, https://doi.org/10.5194/os-14-1093-2018, 2018.

MacLachlan, C., Arribas, A., Peterson, K. A., Maidens, A., Fereday, D., Scaife, A. A., Gordon, M., Vellinga, M., Williams, A., Comer, R. E., Camp, J., Xavier, P., and Madec, G.: Global Seasonal forecast system version 5 (GloSea5): a high-resolution seasonal forecast system, Q. J. Roy. Meteor. Soc., 141, 1072–1084, https://doi.org/10.1002/qj.2396, 2015.

Madec, G. and Imbard, M.: A global ocean mesh to overcome the North Pole singularity, Clim. Dynam., 12, 381–388, https://doi.org/10.1007/BF00211684, 1996.

Madec, G., Bourdallé-Badie, R., Chanut, J., Clementi, E., Coward, A., Ethé, C., Iovino, D., Lea, D., Lévy, C., Lovato, T., Martin, N., Masson, S., Mocavero, S., Rousset, C., Storkey, D., Müeller, S., Nurser, G., Bell, M., Samson, G., and Moulin, A.: NEMO ocean engine, Note du Pole de modélisation, Institut Pierre-Simon Laplace (IPSL), France, 27, Zenodo, https://doi.org/10.5281/zenodo.8167700, 2008.

Masumoto, Y. and Yamagata, T.: Seasonal variations of the Indonesian throughflow in a general ocean circulation model, J. Geophys. Res., 101, 12287–12293, 1996.

Mayer, M. and Alonso Balmaseda, M.: Indian Ocean impact on ENSO evolution 2014–2016 in a set of seasonal forecasting experiments, Clim. Dynam., 56, 2631–2649, https://doi.org/10.1007/s00382-020-05607-6, 2021.

Mayer, M., Balmaseda, M. A., and Haimberger, L.: Unprecedented 2015/2016 Indo-Pacific heat transfer speeds up tropical Pacific heat recharge, Geophys. Res. Lett., 45, 3274–3284, https://doi.org/10.1002/2018GL077106, 2018.

Mayer, M., Tietsche, S., Haimberger, L., Tsubouchi, T., Mayer, J., and Zuo, H.: An Improved Estimate of the Coupled Arctic Energy Budget, J. Clim., 32, 7915–7934, https://doi.org/10.1175/JCLI-D-19-0233.1, 2019.

Mayer, M., Tsubouchi, T., von Schuckmann, K., Seitner, V., Winkelbauer, S., and Haimberger, L.: Atmospheric and oceanic contributions to observed Nordic Seas and Arctic Ocean heat content variations 1993–2020, in: Copernicus Ocean State Report, Issue 6, J. Oper. Oceanogr., 15, 20–28, https://doi.org/10.1080/1755876X.2022.2095169, 2022.

Mogensen, K., Balmaseda, M., and Weaver, A.: The NEMOVAR ocean data assimilation system as implemented in the ECMWF ocean analysis for System 4, https://www.ecmwf.int/file/23284/download?token=L2fInOlQ (last access: 28 May 2022), 2012.

Molcard, R., Fieux, M., and Ilahude, A.: The Indo-Pacific Throughflow in the Timor Passage, J. Geophys. Res., 1011, 12411–12420, https://doi.org/10.1029/95JC03565, 1996.

Molcard, R., Fieux, M., and Syamsudin, F.: The throughflow within Ombai Strait, Deep-Sea Res. Pt. I, 48, 1237–1253, https://doi.org/10.1016/S0967-0637(00)00084-4, 2001.

Nieva Tamasiunas, M., Shinoda, T., Susanto, R. D., Zamudio, L., and Metzger, J.: Intraseasonal variability of the Indonesian throughflow associated with the Madden-Julian Oscillation, Deep-Sea Res. Pt. II, 193, 104985, https://doi.org/10.1016/j.dsr2.2021.104985, 2021.

Nieves, V., Willis, J. K., and Patzert, W. C.: Recent hiatus caused by decadal shift in Indo-Pacific heating, Science, 349, 532–535, https://doi.org/10.1126/science.aaa4521, 2015.

NOAA Physical Sciences Laboratory: Nino 3.4 SST Index, NOAA [data set], https://psl.noaa.gov/gcos_wgsp/Timeseries/Data/nino34.long.data (last access: 7 August 2023), 2003.

Oort, A. and Yienger, J.: Observed Interannual Variability in the Hadley Circulation and Its Connection to ENSO, J. Clim., 9, 2751–2767, https://doi.org/10.1175/1520-0442(1996)009<2751:OIVITH>2.0.CO;2, 1996.

Palmer, M. D., Roberts, C. D., Balmaseda, M., Chang, Y.-S., Chepurin, G., Ferry, N., Fujii, Y., Good, S. A., Guinehut, S., Haines, K., Hernandez, F., Köhl, A., Lee, T., Martin, M. J., Masina, S., Masuda, S., Peterson, K., Storto, A., Toyoda, T., Valdivieso, M., Vernieres, G., Wang, O., and Xue, Y.: Ocean heat content variability and change in an ensemble of ocean reanalyses, Clim. Dynam., 49, 909–930, https://doi.org/10.1007/s00382-015-2801-0, 2017.

Pietschnig, M., Mayer, M., Tsubouchi, T., Storto, A., Stichelberger, S., and Haimberger, L.: Volume and temperature transports through the main Arctic Gateways: A comparative study between an ocean reanalysis and mooring-derived data, Ocean Sci. Discuss. [preprint], https://doi.org/10.5194/os-2017-98, 2017.

Piola, A. and Gordon, A. L.: Pacific and Indian Ocean Upper-Layer Salinity Budget, J. Phys. Oceanogr., 14, 747–753, https://doi.org/10.1175/1520-0485(1984)014<0747:PAIOUL>2.0.CO;2, 1984.

Potemra, J., Hautala, S., and Sprintall, J.: Vertical structure of Indonesian throughflow in a large-scale model, Deep-Sea Res. Pt. II, 50, 2143–2161, https://doi.org/10.1016/S0967-0645(03)00050-X, 2003.

Potemra, J. T. and Schneider, N.: Interannual variations of the Indonesian Throughflow, J. Geophys. Res., 112, C05035, https://doi.org/10.1029/2006JC003808, 2007.

Pujiana, K., McPhaden, M. J., Gordon, A. L., and Napitu, A.: Unprecedented Response of Indonesian Throughflow to Anomalous Indo-Pacific Climatic Forcing in 2016, J. Geophys. Res.-Ocean., 124, 3737–3754, https://doi.org/10.1029/2018JC014574, 2019.

Schönau, M. C., Rudnick, D. L., Cerovecki, I., Gopalakrishnan, G., Cornuelle, B. D., McClean, J. L., and Qiu, B.: The Mindanao Current: Mean structure and connectivity, Oceanography, 28, 34–45, https://doi.org/10.5670/oceanog.2015.79, 2015.

Sprintall, J., Gordon, A. L., Murtugudde, R., and Susanto, R. D.: A semiannual Indian Ocean forced Kelvin wave observed in the Indonesian seas in May 1997, J. Geophys. Res., 105, 17217–17230, https://doi.org/10.1029/2000JC900065, 2000.

Sprintall, J., Wijffels, S., Gordon, A. L., Ffield, A., Molcard, R., Susanto, R. D., Soesilo, I., Sopaheluwakan, J., Surachman,

Y., and Aken, H. M.: INSTANT: A new international array to measure the Indonesian Throughflow, EOS, 85, 369–376, https://doi.org/10.1029/2004EO390001, 2004.

Sprintall, J., Wijffels, S. E., Molcard, R., and Jaya, I.: Direct estimates of the Indonesian Throughflow entering the Indian Ocean: 2004–2006, J. Geosphys. Res.-Ocean., 114, C07001, https://doi.org/10.1029/2008JC005257, 2009.

Sprintall, J., Gordon, A., Koch-Larrouy, A., Lee, T., Potemra, J. T., Pujiana, K., and Wijffels, S. E.: The Indonesian seas and their role in the coupled ocean-climate system, Nat. Geosci., 7, 487–492, https://doi.org/10.1038/ngeo2188, 2014.

Storto, A. and Masina, S.: C-GLORSv5: an improved multipurpose global ocean eddy-permitting physical reanalysis, Earth Syst. Sci. Data, 8, 679–696, https://doi.org/10.5194/essd-8-679-2016, 2016.

Trenberth, K. E.: The Definition of El Niño, Bull. Am. Meteorol. Soc., 78, 2771–2778, https://doi.org/10.1175/1520-0477(1997)078<2771:TDOENO>2.0.CO;2, 1997.

Ummenhofer, C. C., Biastoch, A., and Böning, C. W.: Multidecadal Indian Ocean Variability Linked to the Pacific and Implications for Preconditioning Indian Ocean Dipole Events, J. Clim., 30, 1739–1751, https://doi.org/10.1175/JCLI-D-16-0200.1, 2017.

Uotila, P., Goosse, H., Haines, K., Chevallier, M., Barthélemy, A., Bricaud, C., Carton, J., Fučkar, N., Garric, G., Iovino, D., Kauker, F., Korhonen, M., Lien, V., Marnela, M., Massonnet, F., Mignac, D., Peterson, K. A., Sadikni, R., Shi, L., Tietsche, S., Toyoda, T., Xie, J., and Zhang, Z.: An assessment of ten ocean reanalyses in the polar regions, Clim. Dynam., 52, 1613–1650, https://doi.org/10.1007/s00382-018-4242-z, 2019.

Van Aken, H. M., Brodjonegoro, I. S., and Jaya, I.: The deep water motion through the Lifamatola Passage and its contribution to the Indonesian Throughflow, Deep-Sea Res., 56, 1203–1216, https://doi.org/10.1016/j.dsr.2009.02.001, 2009.

Van Riel, P. M.: The Snellius Expedition in the Eastern Part of the East Indian Archipelago 1929–1930, Vol. II, 5, Leiden, 1956.

Vranes, K., Gordon, A. L., and Ffield, A.: The heat transport of the Indonesian throughflow and implications for the Indian Ocean Heat Budget, Deep-Sea Res. Pt. II, 49, 1391–1410, https://doi.org/10.1016/S0967-0645(01)00150-3, 2002.

Wyrkti, K.: An equatorial jet in the Indian Ocean, Science, 181, 262–264, https://doi.org/10.1126/science.181.4096.262, 1973.

Wyrtki, K.: Physical Oceanography of the Southeast Asian waters, UC San Diego: Library – Scripps Digital Collection, https://escholarship.org/uc/item/49n9x3t4 (last access: 6 July 2022), 1961.

Wyrtki, K.: Indonesian Throughflow and the associated pressure gradient, J. Geophys. Res., 92, 12941–12946, https://doi.org/10.1029/JC092iC12p12941, 1987.

Wyrtki, K. and Kendall, R.: Transports of Pacific equatorial countercurrent, J. Geophys. Res., 72, 2073–2076, https://doi.org/10.1029/JZ072i008p02073, 1967.

Zuo, H., Balmaseda, M., and Mogensen, K.: The new eddy-permitting ORAP5 ocean reanalysis: description, evaluation and uncertainties in climate signals, Clim. Dynam., 49, 791–811, https://doi.org/10.1007/s00382-015-2675-1, 2015.

Zuo, H., Balmaseda, M. A., de Boisseson, E., Tietsche, S., Mayer, M., and de Rosnay, P.: The ORAP6 ocean and sea-ice reanalysis: description and evaluation, EGU General Assembly 2021, online, 19–30 Apr 2021, EGU21-9997, https://doi.org/10.5194/egusphere-egu21-9997, 2021.